HHS Public Access

Author manuscript

Cell Rep. Author manuscript; available in PMC 2024 June 24.

Published in final edited form as:

Cell Rep. 2024 May 28; 43(5): 114156. doi:10.1016/j.celrep.2024.114156.

ER-associated degradation adapter Sel1L is required for CD8+ T cell function and memory formation following acute viral infection

Luis O. Correa-Medero[1], **Shayna E. Jankowski**[2], **Hanna S. Hong**[1], **Nicholas D. Armas**[1], **Aditi I. Vijendra**[2], **Mack B. Reynolds**[1], **Garrett M. Fogo**[3], **Dominik Awad**[4], **Alexander T. Dils**[5], **Kantaro A. Inoki**[2], **Reid G. Williams**[1], **Annabelle M. Ye**[2], **Nadezhda Svezhova**[7,8], **Francisco Gomez-Rivera**[1], **Kathleen L. Collins**[7,8,9], **Mary X. O'Riordan**[8], **Thomas H. Sanderson**[4,10], **Costas A. Lyssiotis**[4,6], **Shannon A. Carty**[5,6,11,*]

[1]Graduate Program in Immunology, University of Michigan, Ann Arbor, MI 48109, USA

[2]University of Michigan, Ann Arbor, MI 48109, USA

[3]Neuroscience Graduate Program, University of Michigan Medical School, Ann Arbor, MI 48109, USA

[4]Department of Molecular and Integrative Physiology, University of Michigan, Ann Arbor, MI 48109, USA

[5]Division of Hematology and Oncology, Department of Internal Medicine, University of Michigan, Ann Arbor, MI 48109, USA

[6]Rogel Cancer Center, University of Michigan, Ann Arbor, MI 48109, USA

[7]Department of Internal Medicine, University of Michigan, Ann Arbor, MI 48109, USA

[8]Department of Microbiology and Immunology, University of Michigan, Ann Arbor, MI 48109, USA

[9]Cellular and Molecular Biology Graduate Program, University of Michigan, Ann Arbor, MI 48109, USA

[10]Department of Emergency Medicine, University of Michigan Medical School, Ann Arbor, MI 48109, USA

[11]Lead contact

*Correspondence: scarty@umich.edu.

AUTHOR CONTRIBUTIONS

L.O.C.-M. and S.A.C. conceived, designed, and guided the research, and wrote the manuscript. L.O.C.-M., S.E.J., H.S.H., N.D.A., A.I.V., M.B.R., G.M.F., D.A., A.T.D., R.G.W., K.A.I., A.M.Y., N.S., F.G.-R., K.L.C., M.X.O., T.H.S., C.A.L., and S.A.C. provided key reagents, performed experiments, and/or analyzed data. T.H.S., C.A.L., and S.A.C. provided expertise in experimental design and data interpretation. S.A.C. supervised the work.

DECLARATION OF INTERESTS

In the past three years, C.A.L. has consulted for Astellas Pharmaceuticals, Odyssey Therapeutics, Third Rock Ventures, and T-Knife Therapeutics and is an inventor on patents pertaining to Kras-regulated metabolic pathways, redox control pathways in pancreatic cancer, and therapeutically targeting the GOT1-ME1 pathway (US Patent no. 2015126580-A1, 05/07/2015; US Patent no. 20190136238, 05/09/2019; International Patent no. WO2013177426-A2, 04/23/2015).

SUPPLEMENTAL INFORMATION

Supplemental information can be found online at https://doi.org/10.1016/j.celrep.2024.114156.

SUMMARY

The maintenance of antigen-specific $CD8^+$ T cells underlies the efficacy of vaccines and immunotherapies. Pathways contributing to $CD8^+$ T cell loss are not completely understood. Uncovering the pathways underlying the limited persistence of $CD8^+$ T cells would be of significant benefit for developing novel strategies of promoting T cell persistence. Here, we demonstrate that murine $CD8^+$ T cells experience endoplasmic reticulum (ER) stress following activation and that the ER-associated degradation (ERAD) adapter Sel1L is induced in activated $CD8^+$ T cells. Sel1L loss limits $CD8^+$ T cell function and memory formation following acute viral infection. Mechanistically, Sel1L is required for optimal bioenergetics and c-Myc expression. Finally, we demonstrate that human $CD8^+$ T cells experience ER stress upon activation and that ER stress is negatively associated with improved T cell functionality in T cell-redirecting therapies. Together, these results demonstrate that ER stress and ERAD are important regulators of T cell function and persistence.

Graphical Abstract

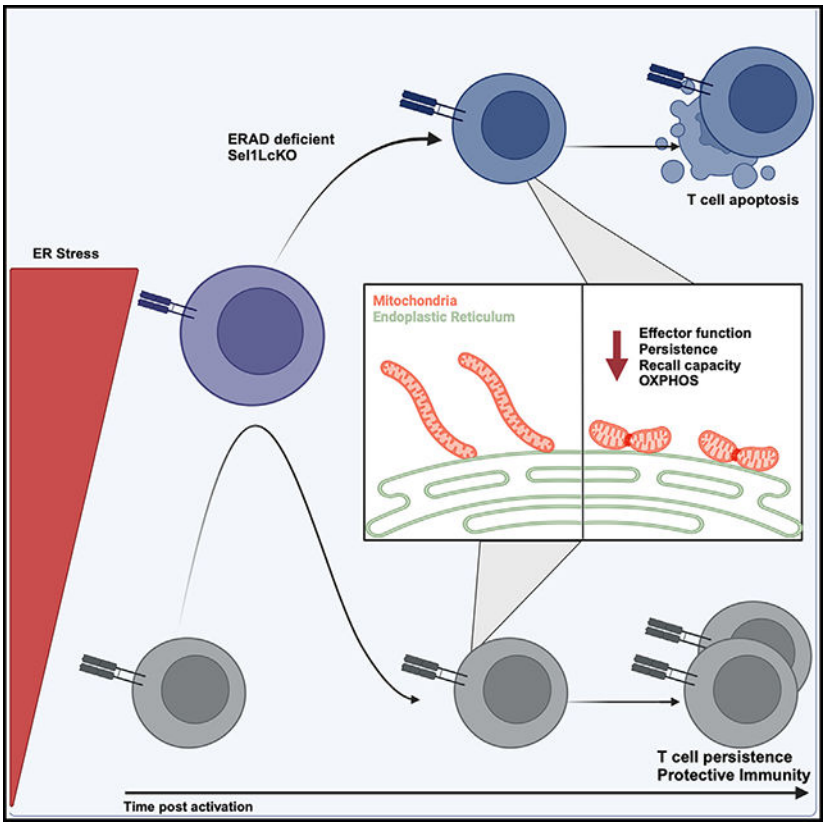

In brief

Correa-Medero et al. report that $CD8^+$ T cells undergo dynamic ER stress during an acute viral infection, and they demonstrate a cell-intrinsic role for Sel1L, the ER-associated degradation adaptor, in $CD8^+$ T cell effector function, persistence, and optimal cellular metabolism.

INTRODUCTION

Following T cell receptor (TCR)-mediated recognition of cognate antigen, naive $CD8^+$ T cells are activated, undergo rapid clonal expansion, and acquire effector function, including cytokine and cytotoxic molecule production, to eliminate intracellular pathogens and tumors.[1–3] After the peak of expansion, the majority of the responding $CD8^+$ T cells become terminally differentiated and undergo cell death following antigen clearance; however, a small fraction of antigen-specific cells persists as memory $CD8^+$ T cells, providing long-lived immune protection by rapidly responding upon antigen rechallenge.[4,5]

As a consequence of TCR-mediated activation, antigen-specific $CD8^+$ T cells undergo dramatic transcriptional, epigenetic, metabolic, and proteomic changes that endow proper function and differentiation.[6–8] Initial work demonstrated that although naive murine $CD8^+$ T cells had relatively low protein synthesis, antigen-specific $CD8^+$ T cells experience the greatest levels of translation at day 5 after acute viral infection, followed by a significant reduction by day 8 post infection (p.i.).[9] In both human and murine T cells, sophisticated proteomic studies corroborated the transition from low basal translation in naive cells to a marked increase in protein synthesis in activated cells.[10–15] Translation is the most error-prone step in gene expression with 10%–30% of all newly synthesized proteins being ubiquitinated and targeted for degradation[16,17]; thus, the question arises as to how cells handle this increase in misfolded protein. Both elevated demand for protein folding and increases in misfolded proteins have been shown to trigger endoplasmic reticulum (ER) stress, whose resolution or failure to resolve has important consequences in cell fate and survival across various cell types.[18,19]

Several studies have started to dissect how maintenance of protein homeostasis and ER stress may regulate $CD8^+$ T cell fate and function. The reduction of proteasome activity early in $CD8^+$ T cell differentiation promoted terminal differentiation, whereas enhanced proteasomal activity led to the promotion of memory characteristics in $CD8^+$ T cells,[20] raising the question of whether ER stress resulting from accumulated misfolded proteins following proteasomal inhibition blocks $CD8^+$ T cell memory formation. Two pathways known to mediate clearance of misfolded protein and thus alleviate ER stress are the unfolded protein response (UPR) and ER-associated degradation (ERAD) pathways. Several groups have studied the role of UPR pathways in $CD8^+$ T cell differentiation and in multiple settings found that UPR activation is associated with terminal differentiation and T cell dysfunction, while deletion of UPR components enhanced T cell function.[21–23] However, very little is known about the role of ERAD in $CD8^+$ T cell fate and function.

Sel1L acts as an adaptor of the ERAD complex, recognizing misfolded proteins in the ER and recruiting them to be translocated to the cytosol for proteasomal degradation.[24] Sel1L also binds and stabilizes Hrd1, the E3 ubiquitin ligase of the ERAD complex.[25] In various cell types, ERAD has been shown to be critical in maintaining ER homeostasis by selectively degrading misfolded protein. Loss of this function then results in disrupted homeostasis manifesting in cell death, altered differentiation, and mitochondrial dysfunction.[25–35] ERAD via Hrd1 deletion is known to regulate $CD4^+$ T cell differentiation, survival, and cytokine production *in vitro* and *in vivo*.[36,37] We and others have demonstrated

that Sel1L is necessary for naive T cell homeostasis.[38,39] How $CD8^+$ T cells manage stresses associated with activation and the role of Sel1L/ERAD are unknown.

We sought to understand the role of ER stress in $CD8^+$ T cell function and persistence following an acute viral infection. Utilizing *in vitro* and *in vivo* models of antigen-specific $CD8^+$ T cell differentiation, we found that T cell activation is associated with a transient induction of ER stress, UPR signaling, and Sel1L expression. Loss of Sel1L, a critical ERAD component, resulted in impaired effector molecule production and memory formation of antigen-specific $CD8^+$ T cells following acute viral infection in a cell-intrinsic manner. Mechanistically, we found that Sel1L/ERAD was required for antigen-specific $CD8^+$ T cell oxidative metabolism, mitochondrial fusion, and c-Myc expression, which are important for $CD8^+$ T memory. Furthermore, we found that ER stress is upregulated following activation of human $CD8^+$ T cells and is associated with terminal differentiation, while alleviation of ER stress is associated with improved $CD8^+$ T cell persistence and function in T cell immunotherapies. Our findings demonstrate a critical role of Sel1L/ERAD in promoting $CD8^+$ T cell effector function and persistence.

RESULTS

Activated $CD8^+$ T cells experience ER stress

As human and murine $CD8^+$ T cells are activated, they quickly upregulate protein synthesis, increase total protein content, and remodel their proteome.[9,11–13,40] However, it is unclear whether this rapid increase in translation induces ER stress. To answer this question, we serially characterized readouts of ER stress in $CD8^+$ T cells using a well-characterized model of *in vitro* differentiation.[41,42] In this system, splenocytes from wild-type (WT) TCR transgenic mice, which have $CD8^+$ T cells expressing the TCR transgene recognizing the lymphocytic choriomeningitis virus (LCMV) epitope glycoprotein (gp) 33–41 (P14 cells), are activated with LCMV gp33–41 peptide in the presence of interleukin-2 (IL-2) for 3 days, after which isolated activated P14 $CD8^+$ T cells (T_{ACT}) were differentiated into IL-2 "effector" cells (IL-2 T_E) or IL-15 "memory" cells (IL-15 T_M) for an additional 3 days (Figure 1A). Since an increase in ER size has been correlated with ER stress,[43,44] we used immunofluorescent staining for calreticulin, an ER-resident chaperone,[45] to quantitate ER size in $CD8^+$ T cells over the course of differentiation. Confocal microscopy demonstrated an increase in calreticulin in T_{ACT} cells relative to naive cells (Figure 1B), which is consistent with other reports that TCR activation increases ER size in T cells.[46] However, because an increase in ER size could also correlate with increased translation, we examined other ER stress measures. When misfolded proteins accumulate in the cell, they form protein aggresomes,[47] which can be detected by the fluorescent dye PROTEOSTAT. To measure proteome quality over the course of differentiation, we measured the cellular levels of misfolded protein aggregates using PROTEOSTAT by flow cytometry and lysine-48-linked ubiquitination (K48-Ub), which is sufficient to target damaged or misfolded proteins for proteasomal degradation,[48] by immunoblotting. Activation of P14 cells was associated with a significant increase in misfolded protein in T_{ACT} cells that partially resolved over time (Figure 1C). We found that T_{ACT} cells consistently contained the highest amount of K48-Ub compared to naive T cells, IL-2 T_E, or IL-15 T_M cells (Figure 1D).

The increase in ER size, protein aggresomes and K48-Ub levels following $CD8^+$ T cell activation suggest an increase in ER stress. In the setting of increased ER stress, the highly conserved UPR pathway is activated to either restore homeostatic balance or trigger apoptosis if cellular stress is unable to be relieved.[18] The UPR employs three distinct ER-bound proteins (inositol-requiring enzyme 1a [IRE1a], activating transcription factor 6 [ATF6], and PKR-like ER kinase [PERK]) that sense unfolded protein in the ER and activate distinct transcriptional programs to resolve stress or execute apoptosis.[18] We performed western blots for representative members of the UPR pathway. PERK activity can be measured by the induction of ATF4 expression, and IRE1a activity can be measured by XBP1 splicing.[49,50] As predicted and in agreement with previous findings,[22,51] the transition from naive to T_{ACT} was associated with increased ATF4 expression and spliced XBP1 (XBP1s)/unspliced XBP1 ratio (Figure 1E). XBP1s induction was orthogonally validated by intracellular flow cytometry (Figure 1F). Together, these data suggest that $CD8^+$ T cells experience ER stress and UPR induction after activation *in vitro*.

Antigen-specific $CD8^+$ T cells experience dynamic ER stress *in vivo*

We next tested whether differentiating $CD8^+$ T cells experience dynamic ER stress *in vivo*. Araki and colleagues[9] demonstrated that translation is highest in antigen-specific $CD8^+$ T cells at day 5 following LCMV-Armstrong acute viral infection. Based on these data, we hypothesized that antigen-specific $CD8^+$ T cells would have the highest levels of ER stress at this time point. Re-analysis of a single-cell atlas consisting of antigen-specific $CD8^+$ T cells responding to LCMV-Armstrong over time[52] corroborated that hallmark signature for UPR was enriched at days 4–5 p.i. (Figure 2A), suggesting that virus-specific $CD8^+$ T cells may experience dynamic ER stress during the course of early activation and differentiation *in vivo*.

To confirm experimentally the transient ER stress experienced by antigen-specific $CD8^+$ T cells, WT mice were infected with LCMV-Armstrong asynchronously. ER stress markers were measured in LCMV-specific $CD8^+$ T cells at days 5 and 8 p.i. and compared to naive $CD8^+$ T cells from uninfected mice. While naive cells contained the lowest amount of protein aggresomes, gp33-specific $CD8^+$ T cells on day 5 p.i. had a 2-fold increase in PROTEOSTAT staining that was reduced to 1.5-fold by day 8 p.i. relative to uninfected naive cells (Figure 2B), suggesting that misfolded proteins peak in viral-specific $CD8^+$ T cells around day 5 p.i. To examine changes in ER size, we used ER Tracker, a flow-cytometric reagent that measures a volumetric readout of ER size, which may serve as a surrogate readout for ER stress.[43,53] Antigen-specific $CD8^+$ T cells on day 5 p.i. had a 4-fold increase ER volume compared to naive cells, which subsequently subsided to baseline by day 8 p.i. (Figure 2C).

Since UPR pathways are activated in response to ER stress,[18] we measured intracellular expression of two UPR transcription factors, the PERK target C/EBP homologous protein (CHOP) and the IRE1a target XBP1s, in LCMV-specific $CD8^+$ T cells. Tetramers against immunodominant peptides gp33–41 and nucleoprotein 396–404 (NP396–404) were used to generalize findings beyond one reactive population. Consistent with our prior data and others,[22,51] expression of UPR factors peaked in LCMV-specific $CD8^+$ T cells on day 5

compared to uninfected naive cells and returned to baseline levels by day 8 in both LCMV-specific populations (Figures 2D and 2E). Together, our data demonstrate that activated $CD8^+$ T cells experience dynamic ER stress during differentiation following an acute viral infection.

Sel1L is upregulated in activated $CD8^+$ T cells

Dynamic ER stress experienced by antigen-specific $CD8^+$ T cells suggests that pathways regulating ER stress responses will be critical to $CD8^+$ T cell differentiation and function. Elegant work has demonstrated that UPR activity diminishes T cell function and persistence, suggesting that enhanced ER stress is detrimental.[21,23,51,54] Similarly, proteosome activity enhances $CD8^+$ T cell persistence while loss of proteosome function limits persistence and memory formation.[20,55] Sel1L, a critical component of ERAD, has been demonstrated to be indispensable for maintaining ER homeostasis and survival in other cell types.[25–29,33,56] However, nothing is known about the cell-intrinsic role of Sel1L/ERAD in activated $CD8^+$ T cells; thus, we sought to elucidate its role in $CD8^+$ T cell fate. First, we examined Sel1L protein expression and found that it increased significantly following activation and was maintained in both IL-2 T_E and IL-15 T_M during *in vitro* differentiation (Figure 3A). In a similar fashion, Sel1L protein expression was upregulated in $gp33^+$ and $NP396^+CD8^+$ T cells on day 8 p.i. relative to naive cells from uninfected controls (Figure 3B). Together, these data demonstrate that Sel1L is induced in $CD8^+$ T cells after antigen encounter.

Sel1L/ERAD is required for optimal $CD8^+$ T cell effector function

Recently we demonstrated that antigen-specific responses to *Listeria monocytogenes* (LM) were impaired in Sel1L conditional knockout (KO) ($Sel1L^{fl/fl}CD4Cre$; Sel1LcKO) mice[38]; we now sought to investigate whether impairment to acute bacterial infection in Sel1LcKO mice was generalizable to viral infection. Utilizing the LCMV-Armstrong experimental system, we find that Sel1LcKO mice experience equivalent viral LCMV burden at day 8 p.i. as measured by RNA levels[57] (Figure S1A). At memory time points, Sel1LcKO mice have reduced formation of LCMV-specific $CD8^+$ T cells (Figure S1B). To assess memory function, equal numbers of $gp33^+$ $CD8^+$ T cells from WT or Sel1LcKO mice previously infected with LCMV were transferred into congenic hosts. Host mice were subsequently infected with *Listeria monocytogenes* engineered to express the LCMV epitope gp33 (LM-gp33). Five days after LM-gp33 infection, we noted a decreased frequency of transferred Sel1LcKO $gp33^+$ cells in the peripheral blood mononuclear cells (PBMCs) and spleen relative to WT controls (Figure S1C and S1D). Measurements of liver Listeria bacterial burden on day 5 p.i. demonstrated increased bacterial load in the mice that received Sel1LcKO memory cells compared to those that received WT memory cells (Figure S1E). These data support a cell-intrinsic role for Sel1L in memory $CD8^+$ T cell protective function; however, deriving conclusions on Sel1L's role in $CD8^+$ T cell-mediated immunity in this system is confounded by the severe lymphopenia and lack of Sel1L expression in both $CD4^+$ and $CD8^+$ T cells in the Sel1LcKO mice.[38]

Thus, to interrogate the cell-intrinsic role of Sel1L, we generated Sel1LcKO mice that express the transgenic P14 TCR (Sel1LcKO P14). At baseline, Sel1LcKO P14 mice had comparable frequencies and absolute numbers of peripheral T cell populations as WT P14

littermates (Figure S2A), as well as similar expression of naive markers CD62L and CD127 (Figure S2B). Sel1LcKO P14 cells did not have detectable ER stress as measured by ER size, PROTEOSTAT, CHOP, and XBP1s expression compared to WT P14 cells (Figure S2C). Following *in vitro* activation with cognate peptide in the presence of splenic antigen-presenting cells, Sel1LcKO P14 cells upregulated TCR activation markers CD25 and CD69 at a similar frequency and to similar levels as WT P14 cells (Figure S2D), indicating no alterations in early TCR signaling or activation. Together, these data suggest that Sel1L deficiency does not alter T cell homeostasis or TCR activation in Sel1LcKO mice expressing a fixed TCR.

To determine the cell-intrinsic role of Sel1L/ERAD in $CD8^+$ T cell function, we transferred congenically disparate WT P14 and Sel1LcKO P14 cells mixed in a 1:1 ratio into congenic recipient B6.SJL mice that were subsequently infected with LCMV-Armstrong. Eight days p.i., stimulation of splenocytes with gp33–41 was performed to assess effector molecule expression. Intracellular staining revealed a significant decrease in cytokine double (interferon-γ [IFN-γ]$^+$, tumor necrosis factor a [TNF-α]$^+$) as well as polyfunctional producers (i.e., production of multiple cytokines) in Sel1LcKO P14 (Figure 4A); importantly, polyfunctional $CD8^+$ T cells have been associated with superior control of viral infections.[58,59] Loss of double polyfunctional cells appeared to primarily be driven by lack of TNF-α-expressing cells as the frequency of IFN-γ-expressing cells was not significantly altered. However, on a per-cell basis, cytokine-producing cells had both lower IFN-γ and TNF-α expression. To examine global effector molecule co-expression, we performed SPICE analysis[60] on the stimulated WT and Sel1L-deficient P14 cells and found that WT cells consistently were more able to co-express 4–5 effector molecules than Sel1LcKO cells (Figure 4B). Together, these data demonstrate that Sel1L/ERAD is essential for optimal $CD8^+$ T cell function in a cell-intrinsic manner.

Sel1L/ERAD is required for $CD8^+$ T cell survival and memory formation

Resolution of ER stress is critical for cell survival, and loss of Sel1L in other cell types has been associated with cell death and dysfunction. Limited T cell persistence is a barrier to more efficacious immunotherapeutics; however, pathways contributing to limited T cell persistence are not fully understood. The transient ER stress as well as the selective induction of Sel1L in antigen-experienced cells suggested that Sel1L/ERAD would be necessary for persistence of antigen-specific $CD8^+$ T cells during acute viral infections. We co-transferred equal numbers of congenically distinct WT P14 and Sel1LcKO P14 into B6.SJL mice and subsequently infected them with LCMV-Armstrong. At day 5 p.i., Sel1LcKO P14 donor cells moderately outcompeted WT P14 donors (Figure S3A) with no alteration in differentiation or apoptosis (Figure S3B and S3C). Sel1LcKO P14 donor cells had significantly reduced CD25 expression (Figure S3D). Examination of UPR activation revealed no differences in Sel1LcKO P14 relative to transferred WT P14 cells (Figures S3E and S3F). Together, these data demonstrate that Sel1L/ERAD was not required for initial T cell expansion or the maintenance of protein homeostasis at day 5 p.i. In contrast, by day 8 p.i., the Sel1LcKO P14 population had reduced frequency in the spleen, lymph nodes, and blood compared to the WT P14 population (Figure 5A), suggesting that Sel1L was required for later stages of antigen-specific $CD8^+$ T cell survival and expansion.

To determine whether this alteration in frequency was due to decreased proliferation or increased cell death, we performed Ki67 staining and 7-aminoactinomycin D (7-AAD)/ Annexin V staining. Despite being found at slightly higher frequencies than WT at day 5 p.i. (Figure S3A), Sel1LcKO P14 expressed marginally lower levels of the proliferation marker Ki67 compared to WT on day 8 p.i. (Figure 5B). Apoptosis as measured by Annexin V and 7-AAD staining suggest that Sel1LcKO P14 die at a greater rate than WT P14 cells at day 8 p.i. (Figure 5C). Although both proliferation and apoptosis were statistically significantly altered in the setting of Sel1L loss, the magnitude of apoptosis differences exceeded the minor difference in proliferation, suggesting that Sel1L is necessary primarily to safeguard virus-specific $CD8^+$ T cells from apoptosis at the peak of expansion following an acute viral infection.

During acute viral responses, $CD8^+$ T cells differentiate into heterogeneous cell states with different memory potential, which can be identified by different cell-surface proteins and different canonical transcription factors. Phenotypically, terminal effector (TE) cells express high surface expression of killer cell lectin-like receptor G1 (KLRG1) and low expression of the interleukin-7 receptor a (IL7ra; CD127), whereas memory precursor (MP) cells express high levels of CD127 and low KLRG1.[61–63] MP cells primarily seed the memory T cell pool, and TE cells have a significantly reduced capacity to contribute to the long-lived memory T cell pool.[62] Phenotypically, Sel1LcKO P14 cells had TE and MP populations similar to those in WT (Figure 5D). However, Sel1LcKO P14 demonstrated significantly reduced expression of transcription factor TCF1 (Figure 5E), known to be required for $CD8^+$ T cell memory formation and stemness.[64–66] To determine the necessity of Sel1L/ERAD in long-term persistence of viral-specific $CD8^+$ T cells, we longitudinally tracked co-transferred Sel1LcKO and WT P14 cells in the peripheral blood of congenic hosts following LCMV. We observed a steady decrease in the persistence of Sel1LcKO P14 compared to WT over time (Figure 5F). Despite the lack of persistence, Sel1LcKO P14 cells had similar frequencies of central memory (T_{CM}) and effector memory (T_{EM}) subsets[67–69] as WT P14 cells (Figure S4A). Importantly, we noticed variation in the rates of Sel1LcKO P14 persistence in recipient mice at memory time points despite being derived from the same donor. Thus, we sorted donor cells at day 45 p.i. to confirm continued Sel1L deletion. We found that Sel1LcKO P14 cells that persisted at the highest levels no longer had complete Sel1L deletion, suggesting that they expanded from a small population that had initially escaped Cre recombinase deletion (Figure S4B). These data point to a strong selection pressure to maintain Sel1L expression to promote $CD8^+$ T cell survival. Together, these data demonstrate that Sel1L/ERAD is essential for $CD8^+$ T cell persistence in a cell-intrinsic manner following an acute viral infection.

Sel1L regulates $CD8^+$ T cell metabolism

To gain insights into the mechanism whereby Sel1L regulates $CD8^+$ T cell persistence, we performed RNA sequencing (RNA-seq) analysis on Sel1LcKO P14 and WT P14 at day 8 post LCMV infection. Pathway analysis[70] of WT P14 and Sel1LcKO P14 transcriptomes demonstrated that Sel1LcKO P14 cells contained a decrease in terms corresponding to protein synthesis, such as ribosome and rRNA binding, and an increase in terms corresponding to the ER, Golgi apparatus, response to hydrogen peroxide, and

fatty acid metabolism—pathways known to be upregulated in cells experiencing ER stress (Figure 6A).[71] Pathways corresponding to the regulation of apoptosis were also enriched in Sel1LcKO P14, corroborating our previous data. Expression of cytokines Gzmb, IFN-γ, and IL-2 were not altered, suggesting that the cytokine production defect observed above is primarily due to translational defects and not transcription (Figure S5A). Furthermore, immune signature analysis demonstrated that the Sel1LcKO P14 transcriptome was enriched in terms corresponding to terminal differentiation and T cell exhaustion while being depleted in terms corresponding to memory formation (Figure S5B), which corresponds to the data demonstrating lower TCF1 expression and lack of persistence in Sel1L-deficient P14 cells. Additionally, most altered pathways were related to cellular metabolism, with terms corresponding to oxidative phosphorylation such as “respiratory chain complex IV,” “oxidative phosphorylation,” “NADH dehydrogenase activity,” and “mitochondrial respiratory chain complex I” being significantly depleted in Sel1LcKO P14 cells compared to WT (Figure 6A).

Since oxidative phosphorylation (OXPHOS) is known to play a critical role in $CD8^+$ T cell persistence and memory,[42] we focused on determining whether Sel1L regulates $CD8^+$ T cell metabolism. Previous work in brown adipocytes demonstrated that Sel1L deletion impaired mitochondrial OXPHOS by altering mitochondria morphology and accumulation.[34] To interrogate the role of Sel1L in $CD8^+$ T cell metabolism, we profiled activated WT and Sel1LcKO P14 cells using extracellular flux analysis. Consistent with our RNA-seq data, Sel1L loss impaired OXPHOS with decreased basal and maximal oxygen consumption rate (Figure 6B) compared to WT. Sel1L was also required to maintain spare respiratory capacity, also known as metabolic fitness, a measurement that reflects the reserved energy in cells to respond to stress. Importantly, spare respiratory capacity has been linked to the ability of $CD8^+$ T cells to persist long term *in vivo*.[42] In addition, activated Sel1LcKO P14 cells also had reduced glycolysis as measured by extracellular acidification rate (Figure 6C). To correlate these finding *in vivo*, we examined WT and Sel1LcKO P14 cells directly ex vivo on day 8 p.i. using the cationic dye tetramethylrhodamine methyl ester perchlorate (TMRM) to determine the relative mitochondrial membrane potential of the transferred cells. Reduced mitochondrial membrane potential suggested that Sel1L-deficient P14 cells have reduced OXPHOS capacity while maintaining similar amounts of mitochondria as measured by MitoTracker green (Figures 6D and 6E). Overall, these results demonstrate that Sel1L is required for optimal $CD8^+$ T cell bioenergetic capacity.

Mitochondrial morphology is a critical regulator of a cell’s capacity to undergo oxidative phosphorylation.[72,73] In $CD8^+$ T cells, mitochondrial fusion has been demonstrated as a key checkpoint promoting T cell persistence.[74] We investigated the role of Sel1L in regulating mitochondrial morphology in T cells. In contrast to previous data in adipocytes, where the loss of Sel1L resulted in increased mitochondrial fusion,[34] confocal microscopy of *in vitro* activated Sel1LcKO P14 cells revealed altered mitochondrial morphology with reduced mitochondrial volume, surface area, and length compared to WT (Figure S6A), consistent with increased mitochondrial fission. Mitochondrial fusion and fission is a tightly regulated process in association with mitochondrial-ER contact sites (MERCS).[75,76] There was no difference in expression of the mitochondrial morphology regulators Drp1 and Opa1 (Figure S6B),[74,77,78] so we investigated MERCS formation. Super-resolution microscopy

for ER (KDEL) and mitochondria (TOM20) of WT and Se1lLcKO T_{ACT} cells revealed an increase in ER-associated mitochondria (Figure S6C), consistent with increased MERCS formation in the absence of Sel1L. Future investigation is required to elucidate the direct molecular mechanism by which Sel1L regulates mitochondrial morphology and MERCS formation and to determine the extent to which these changes are required to maintain cellular metabolism.

Given the critical role of c-Myc in orchestrating T cell metabolism,[79,80] we also investigated whether c-Myc expression was altered. Following activation with antigen, Sel1LcKO P14 cells expressed significantly less c-Myc protein compared to WT P14 cells (Figure 6F). Together, these data suggest a possible mechanism by which Sel1L maintains sufficient T cell bioenergetics; however, further investigation will be needed to evaluate relative contributions of these findings.

ER stress in human T cells

Uncovering novel pathways regulating T cell persistence can provide valuable insight into immunotherapy development and may increase the likelihood of therapeutic benefit for patients.[81] After antigen clearance, a minority of T cells persist and acquire memory phenotype in both mice and humans.[82] Memory T cell subsets have distinct capacities for protection against reinfection, severe disease, and therapeutic efficacy.[83–85] Specifically, T stem cell memory (T_{SCM}) cells are considered the least differentiated and contain the largest potential for memory response and generating effector progeny.[86,87] T_{CM} cells retain properties similar to those of T_{SCM} cells but contain reduced stem-like properties. T_{EM} cells behave more as committed progenitor cells, undergoing terminal differentiation after antigen re-encounter[88], and T_{EM} cells that re-express CD45RA (TEMRA) cells represent a subset that is most differentiated and has acquired full effector function. Finally, $PD1^+CD39^+$ cells are putative exhausted T cells that could represent alternative differentiation lineage.[89–91] We sought to determine whether human $CD8^+$ T cell differentiation states were associated with enhancement of gene signatures corresponding to ER stress. Utilizing a published transcriptional dataset of human T cell subsets from healthy donors,[92] we conducted gene set variation analysis and found that terms corresponding to ER stress increased with terminal T cell differentiation (Figure 7A). Given our findings demonstrating that murine T cell activation resulted in induction of ER stress pathways, we asked whether human $CD8^+$ T cells underwent a similar process. Indeed, reanalysis of proteomic data of resting and activated human $CD8^+$ T cell subsets[93] reveals significant upregulation of proteostatic proteins protein disulfide isomerase (PDIA6), PERK, ER stress-induced chaperone BiP, and ER oxidoreductase-1-like (ERO1L) across all subsets after activation (Figure 7B). Interestingly, Sel1L RNA expression was only increased in TEMRA cells relative to naive cells (Figure S7A). While Sel1L protein levels were stable across resting subsets, T cell activation increased the expression of Sel1L protein (Figure S7B). Previous work in other cell types has shown that ERAD gene expression is induced by XBP1 activity,[94–96] and surprisingly there is only a subset-specific correlation of Sel1L expression with XBP1 in human T cells, suggesting the possibility that other transcription factors may control Sel1L expression in T cells (Figure S7C). Next, we sought to corroborate that T cell activation resulted in the accumulation of misfolded protein. Activation of $CD8^+$ T cells from healthy

human donors revealed that activated CD8$^+$ T cells accumulate misfolded protein relative to resting unstimulated cells (Figure 7C). Additionally, activated CD8$^+$ T cells upregulated ER stress marker XBP1s relative to rested cells (Figure 7C).

To investigate the role of ER stress in T cell-based immunotherapies, we examined the relationship of ER stress pathways and T cell fitness in this setting. In the last decade, bispecific antibodies and chimeric antigen receptor T (CAR-T) cell therapy have been approved to treat and potentially cure relapsed/refractory B cell malignancies.[97,98] However, lack of persistence and T cell exhaustion remain roadblocks to optimizing clinical responses for more patients. Bispecific antibodies contain two antibody variable regions, one of which includes anti-CD3, tethered by a linker to a tumor-specific antigen, such as anti-CD19. In a study identifying mechanisms of exhaustion in T cells responding to the anti-CD3 3 anti-CD19 therapy AMG562,[99] the authors found that treatment-free intervals (TFIs) ameliorate T cell exhaustion and improve T cell persistence, cytotoxic function, and metabolic profile compared to continuous exposure to AMG562. Reanalysis of transcriptomic data of the responding T cells demonstrated that continuous stimulation resulted in enhanced ER stress compared to cells that experienced TFIs (Figure 7D). In a separate dataset, CAR-T cells were found to have improved functionality after undergoing rest from CAR stimulation.[100] We posited that reversal of ER stress could be associated with improved CAR-T cell function; indeed, we find that CAR-T cell reinvigoration was associated with reversal of transcriptional signatures corresponding to “response to unfolded protein” (Figure 7E). Together, these data demonstrate that ER stress is induced during human T cell activation and is associated with terminal differentiation, while the reversal of ER stress is associated with improved T cell persistence and function in two T cell-based immunotherapeutic modalities. Future studies are needed to determine causality and elucidate whether modulating ER stress could be sufficient to improve T cell persistence and function in therapeutic settings.

DISCUSSION

Understanding fundamental molecular pathways that regulate CD8$^+$ T cell function and fate are critical to improving T cell-mediated responses to viral infections and cancer as well as identifying novel targets to improve immunotherapies. CD8$^+$ T cell proteome remodeling is known to be dynamically regulated following acute viral infection, with significant amounts of new protein synthesis occurring; however, neither the experience of ER stress nor the cell-intrinsic role of Sel1L/ERAD play in CD8$^+$ T cell fate following viral infection have been explored. Here, we demonstrate that viral-specific murine CD8$^+$ T cells experience transient ER stress during acute viral infection and identify Sel1L/ERAD as necessary for effector function, optimal metabolism, and CD8$^+$ T cell persistence after viral infection. Furthermore, we find that primary human CD8$^+$ T cells experience ER stress following activation and that ER stress is negatively associated with function and persistence in T cell-based immunotherapies.

Thus far, studies of ER stress pathways in T cells have focused primarily on the role of the UPR pathway. Acute bacterial and viral infections were shown to activate the IRE1/XBP1 pathway in CD8$^+$ T cells *in vivo*, with overexpression of XBP1s promoting

terminally differentiated KLRG1$^+$ cells.[22] Both XBP1s and CHOP have been found to have detrimental roles in CD8$^+$ T cell persistence in tumor models, suggesting that signals derived from ER stress limit T cell persistence.[21,23] Protein misfolding and ER stress were not directly studied. It is also apparent that, in situations of chronic misfolded protein, enzymes responsible for clearing misfolded protein can have detrimental effects on cell survival, as evidenced by chemical inhibition of ER oxidoreductase 1α and protein disulfide isomerase, an ER chaperone that promotes protein folding and stability,[101] in murine T cells enhancing cell survival even in settings of chronic ER stress.[51,102] However, orthogonal genetic studies are required to ensure the validity of these findings, as inhibitors of these enzymes have low selectivity and potential off-target effects.[103] The role of proteostatic enzymes and their maladaptation seems to be context dependent, as Fernández-Alfara et al.[104] elegantly demonstrate that that loss of CPEB4, an enzyme required for ER stress adaptation, leads to exacerbated UPR activation and limited T cell persistence and function.

The ERAD pathway mediates the clearance of misfolded protein. In various cell types, including hematopoietic stem cells and CD4$^+$ T cells, ERAD has been shown to be required for cellular homeostasis,[25–27,29–33,105] with the ERAD adaptor Sel1L being ubiquitously expressed across various tissues.[25–35,38,56,105] ERAD loss has cell- and stage-specific implications for cellular function and/or survival[106] as well as cell-specific targets.[107] In T cells, deletion of the ERAD ubiquitin ligase Hrd1 in mature conventional T cells mediated by CD4Cre deletion results in severe lymphopenia with loss of both CD4$^+$ and CD8$^+$ T cells.[108] We and others have reported similar findings utilizing CD4cre-mediated deletion of Sel1L during homeostasis.[38,39] In contrast, Hrd1 deletion in only CD4$^+$ regulatory T cells induced ER stress that limited their stability and immunosuppressive function without impairing survival.[37] In this study, we find that Sel1L protein expression is induced in primary murine CD8$^+$ T cells after TCR-mediated activation *in vitro* and *in vivo*. This upregulation coincides with an increase in ER stress indicators *in vitro* such as K48-ubiquitin and protein aggresome formation as well as upregulation of the UPR factors ATF4 and XBP1s. These data suggest that T cell activation results in ER stress requiring the upregulation of Sel1L along with UPR pathways to maintain ER homeostasis.

Limited persistence of CD8$^+$ T cells is intrinsically correlated with the reduced capacity to perform oxidative metabolism.[42,74,109,110] We demonstrate that Sel1L is required for activated CD8$^+$ T cells to maintain OXPHOS. Several other pathways involved in relieving ER stress have been implicated in OXPHOS regulation in T cells. For instance, proteasomal inhibition results in reduced OXPHOS, while attenuated UPR signaling, through the loss of transcriptional effectors XBP1 or PERK, restores OXPHOS in T cells.[20,51,54] Together these results suggest disrupted ER homeostasis as a possible mechanism for maintaining OXPHOS in T cells, although no unifying molecular mechanism has been identified.

It is well established that mitochondrial dynamics are critical for oxidative metabolism.[73,74,111,112] Our data show that Sel1L loss alters mitochondrial morphology, leading to an increase in smaller (i.e., more fissed) mitochondria and increased MERCS formation. Multiple lines of evidence link chronic ER stress to mitochondrial fission and increased mitochondrial-ER contacts.[75,113] Although we did not identify protein expression differences in the mitochondrial morphology regulators phospho/total Drp1, or Opa1,

intriguingly we did note an increase in MERCS formation in the setting of Sel1L loss. ER tubules have been shown to mediate mitochondrial fission through physical constriction of mitochondrial membranes,[114] raising an intriguing possibility of whether increased MERCS formation is responsible for the mitochondrial fission noted. However, MERCS also serve a wide variety of other cellular functions, including calcium homeostasis and lipid exchange.[75,76,115] Mitochondrial-ER interplay has been increasingly recognized to play key roles in T cell fate and function.[115–117] Thus, additional work to define exactly how ERAD regulates MERCS formation and immunometabolic functions will be critical to understanding how ER homeostasis pathways regulate T cell metabolism.

In our studies, we also noted that c-Myc expression was significantly lower in the setting of Sel1L deficiency. c-Myc is essential for T cell metabolism after activation[79,80,118] and promotes $CD8^+$ T cell persistence.[119,120] In T cells, TCR signaling is known to regulate Myc transcription and c-Myc protein levels,[80,121,122] while IL-2 signaling is required to maintain c-Myc protein levels.[80] Given that CD25 expression (the high-affinity IL-2 receptor) was significantly reduced in Sel1-deficient P14 cells on day 5 p.i. *in vivo*, these observations suggest a possible model whereby Sel1L/ERAD maintains CD25 and c-Myc expression to support the bioenergetic demands of T persistence.

In human $CD8^+$ T cells, we demonstrate that they experience ER stress following TCR-mediated activation, as evidenced by increased protein aggresomes and XBP1s expression. Furthermore, bioinformatics analyses of healthy human donor transcriptomes and proteomes correlate ER stress and UPR activation with terminal differentiation and activation. In recent years, T cell-redirecting immunotherapies, such as CAR-T and bispecific antibodies, have been revolutionizing therapies for patients with relapsed/refractory multiple myeloma, B cell lymphomas, and leukemias[97,123,124] and may provide an effective therapy for some autoimmune diseases.[125] In murine models of adoptive cellular therapy for solid tumors, mitigating ER stress in T cells improves anti-tumor responses.[21,23,54,102] Given that exhaustion and lack of persistence is one of the major hurdles to further improvement of T cell-redirecting therapies,[126] we posited that ER stress may play a role in limiting the efficacy of these therapeutic T cells targeted to hematologic malignancies. Analysis of two publicly available datasets examining approaches to improve CAR-T and bispecific antibody function and persistence found an association between downregulated ER stress pathways and improved persistence/function. These data raise the possibility that ER stress may limit the persistence and/or function of therapeutic T cells; however, this observation could be correlative rather than causative. Mechanistic studies are needed to delineate the role played by ER stress in limiting T cell-redirecting therapies and whether therapeutically alleviating ER stress can improve clinical outcomes.

Maintenance of ER homeostasis is a shared biological necessity across cell types, but the outcomes of ER stress responses vary widely by cell type and biological context. Collectively, our data identify Sel1L/ERAD as an important regulator of $CD8^+$ T cell function and persistence following acute viral infection and highlight the interplay of Sel1L/ERAD and metabolism in maintaining T cell immunity. Future studies are needed to determine whether ERAD and other ER stress pathways are targetable pathways to modulate T cell immunity and improve T cell-based immunotherapies.

Limitations of the study

While we identified that Sel1L/ERAD was required for optimal cellular metabolism, the exact molecular mechanism that underlies this bioenergetic insufficiency remains unclear. We noted several dysregulated pathways including altered mitochondrial dynamics, altered MERCS, and lower c-Myc expression. How Sel1L/ERAD loss directly or indirectly contributes to these findings and the extent to which each contributes to loss of optimal metabolism remains unclear.

Additional limitations are that we noted a fraction of Sel1LcKO cells that undergo Cre escape *in vivo* following acute viral infection. This heterogeneity may have led to less significant *in vivo* results than if we had used a Cre reporter system, as we were measuring bulk population marked by tetramer positivity or peptide reactivity for the *in vivo* experiments.

Additionally, our bioinformatics analysis of redirected human T cells, while intriguing and informative, is limited by the intrinsic correlative nature of such analyses. It is possible that the increased ER stress signatures noted are a result of the repeated antigen receptor stimulation and do not play a causal role in T cell exhaustion or function in T cell immunotherapies.

STAR★METHODS

Detailed methods are provided in the online version of this paper and include the following:

RESOURCE AVAILABILITY

Lead contact—Further information and request for resources and reagents should be directed to and will be fulfilled by the lead contact, Shannon A. Carty (scarty@umich.edu).

Materials availability—This study did not generate new unique reagents.

Data and code availability

- Generated bulk RNA-seq data have been deposited at GEO and are publicly available as of the date of publication. Additionally, this paper utilizes existing, publicly available data. Accession numbers for the datasets are listed in the key resources table and in associated figure legends. Flow cytometry, microscopy, and western blot data are available upon request.
- This paper does not report original code.
- Any additional information required to analyze the data reported in this paper is available from the lead contact upon request.

EXPERIMENTAL MODELS AND STUDY PARTICIPANT DETAILS

Mice—C57BL/6J mice, and CD4Cre^{+} mice were obtained from The Jackson Laboratory and bred at the University of Michigan. B6.SJL-Ptprca (CD45.1^{+}) mice were obtained from The Jackson Laboratory. Sel1L floxed mice[25] were a kind gift from Ling Qi, University

of Virginia. All mice were backcrossed at least ten times to a C57BL/6J background. Sel1L$^{fl/fl}$CD4$^{+/}$Cre were bred to P14[143,144] mice to generate Sel1L$^{fl/fl}$CD4Cre^{+} P14 mice. Control mice for experiments included age-matched P14 Sel1L$^{fl/fl}$, P14 Sel1L$^{+/+}$CD4Cre^{+}, P14 Sel1L$^{fl/fl}$CD4Cre^{-} or C57BL/6J animals. All experiments were performed according to protocols approved by the Institutional Animal Care and Use Committee of the University of Michigan (PRO00009175; PRO00010912). Mice were bred and maintained in specific pathogen-free animal facility (22°C with 40% humidity) on a 12-h dark/12-h light cycle at the University of Michigan. Mice were used 6- to 10-week-old were used at start of experiments, both sexes are represented in the data and no sex differences were noted.

***In vitro* differentiation—**Splenocytes from P14 mice, whose CD8^{+} T cells are >85% P14+, were cultured in T cell medium (10% FBS, 50uM 2-ME, 2mM L-glutamine/penicillin/streptomycin in IMDM) containing 100 ng/ml gp33–41 (Anaspec, cat.# AS-61669, sequence: KAVYNFATC) and 100U/ml recombinant human IL-2 (PeproTech, cat.# 200-02) for 48hrs. After 48hrs of culture, cells were replated in T cell medium containing 100U/ml IL-2 an additional 24hrs. At 72hrs of incubation, CD8^{+} P14 T cells were purified by negative selection using magnetic beads according to the manufacturer's instructions (Biolegend, cat.# 480008). Cells were then cultured for an additional 3 days in T cell medium supplemented with either recombinant IL-2 (100U/ml) or IL-15 (10 ng/ml) (PeproTech, cat.# 210-15). Naive CD8^{+} T cells were purified from total splenocytes at the start of the experiment (Biolegend, cat.# 480044). All cells were cultured in incubator maintained at 37°C with a humidified atmosphere containing 5% CO_2.

Infections and adoptive transfer—Mice were infected with 2×10^5 pore-forming units (p.f.u.) LCMV-Armstrong intraperitoneally (i.p). For experiments on day 5 and day 8 p.i., spleen, lymph nodes and peripheral blood mononuclear cells (PBMCs) were isolated and single cell suspensions were obtained for flow cytometric or other downstream analysis. For longitudinal studies, PBMCs were collected at days 8, 15, 30 and 45 p.i. in a 4% sodium citrate solution. Peripheral blood mononuclear cells were then isolated utilizing a Ficoll-paque gradient (GE Healthcare, cat. # 45-001-749) and stained for flow cytometry. For adoptive co-transfer experiments, 1:1 mix of donor WT P14 (CD45.1/2) and Sel1LcKO P14 (CD45.2) cells was generated and transferred into 2.5×10^3 cells of each donor was co-transferred into congenically disparate mice sex-matched, 6–8 week old B6.SJL (CD45.1) mice. In select day 45 LCMV experiments, donor P14 cells were sorted to confirm lack of Cre escape via RT-PCR and data was excluded if deletion was <50%. For *Listeria monocytogenes* infections, mice were infected with $5.8–9.0 \times 10^4$ colony-forming units (CFU) *Listeria monocytogenes* that expresses the LCMV gp33 epitope (LM-gp33), as indicated and peripheral blood and spleens were collected on day 5p.i. LM-gp33 was grown and bacterial loads were measured as previously described.[145]

Human samples—Anonymized leukocytes isolated by apheresis were obtained from the New York Blood Center, and peripheral blood mononuclear cells (PBMCs) were isolated by Ficoll-Paque Plus (GE Helthcare, cat.# 17144002) centrifugation using SepMate tubes (Stemcell Technologies, cat.#85450) according to the manufacturer's protocol. CD8^{+} lymphocytes were positively selected with Dynabeads according to the manufacturer's

protocol (Invitrogen, cat.#11147D). Isolated $CD8^+$ cells were either rested in 10 ng/ml human IL-7 (PeproTech, cat. # 200-07-10μg) for 3 days or activated using Dynabeads per manufacturer's protocol (Invitrogen, cat. #11131D) in addition with 100 Units/ml human recombinant IL-2 in human T cell media (RPMI, Gibco, cat.# 11875093) supplemented with 50uM beta-mercaptoethanol (Sigma-Aldrich, cat.#M3148-250ML), 2mM L-glutamine/penicillin/streptomycin (Gibco, cat.#10378016), 10% FBS (Cytiva, cat.# SH3039603), and 1x non-essential amino acids (Gibco, cat.# 11140050). Cells were cultured for 3 days before staining and analyzed via flow cytometry. All samples were allocated the same way. Due to the deidentification processes we do not know age, sex ancestry, ethnicity nor socioeconomic status of the donors from which the samples used in this manuscript originated, which may limit the generalizability. All cells were cultured in incubator maintained at 37°C with a humidified atmosphere containing 5% CO_2.

METHOD DETAILS

Flow cytometry and cell sorting—Single cell suspensions from indicated organs were isolated. Cells were washed in FACS buffer (PBS with 2% FBS) and stained with indicated antibodies or dyes. Intracellular staining was performed using a Cytofix/cytoperm kit (BD Biosciences, cat.# BDB554722) or a Foxp3/transcription factor staining buffer set (Invitrogen, cat.# 50-112-8857), according to manufacturer instructions. Live cell discrimination was performed using LIVE/DEAD Aqua stain (Invitrogen, cat.#L34965) according to the manufacturer's instructions. For apoptosis detection, cells were harvested, and after incubation with surface antibodies, cells were washed with Annexin Binding Buffer (Biolegend, cat.# 422201) and incubated with Annexin V (Biolegend, cat.# 640918) and 7AAD (Biolegend, cat.# 420403) for 20 min at room temperature in the dark and immediately analyzed. For flow cytometric cell sorting, $CD8^+$ T cells were purified by negative selection magnetic cell sorting (Biolegend, cat.# 480008). Cells were sorted on FACS Aria. For flow cytometry experiments, data were acquired on BD Fortessa (BD Biosciences) and analyzed using FlowJo (version 10.6 or higher).

Intracellular cytokine detection—For experiments involving *ex vivo* stimulation, splenocytes from LCMV-infected animals at D8 p.i were stimulated with 100 ng/ml gp33 peptide in the presence of Brefeldin A (BD, cat. #BDB555029) according to manufacturer instructions was added to cultures for 4–5 h and then analyzed for intracellular cytokine staining. Boolean gating was used to generate table identifying cells by their ability to produce any combination of cytokines (Granzyme B, IFNγ TNFα, IL2), degranulation maker CD107a or no cytokine production. Files were then imported into SPICE[60] displayed graphs were made using custom R scripts.

Extracellular flux analysis—Seahorse assays were performed using an XF-96 Extracellular Flux Analyzer (Agilent). The day before the assay, sensor cartridges were incubated in dH_2O overnight then hydrated in XF calibrant (Agilent) for 1 h in a non-CO_2 incubator at 37°C on the day of the assay. Following *in vitro* culture, cells were washed and resuspended in XF DMEM media. 2–2.5 × 10^5 cells per well were seeded on poly-L-lysine-coated plates and allowed to equilibrate for 30 min in a non-CO_2 incubator at 37°C. Cartridges were loaded with 1–2μM oligomycin (O), carbonyl

cyanide *p*-trifluoromethoxyphenylhydrazone (FCCP) (1 μM), and 1 μM rotenone/antimycin A (R/A). After the assay, measurements were normalized based on cell seeding density using CyQuant (Invitrogen). Spare respiratory capacity (metabolic fitness) was determined by subtracting basal OCR from maximal OCR measurements.

RNA sequencing and analysis—5×10^4 P14 cells per genotype were sorted from mice on day 8 p.i. of LCMV-Armstrong. After sort, cells were washed thoroughly in PBS followed by RNA extraction utilizing the RNA micro kit (Qiagen, cat. #74004) and removing contaminating genomic DNA utilizing DNase I treatment. Library prep and next-generation sequencing was carried out in the Advanced Genomics Core at the University of Michigan. Briefly, RNA was subjected to strand specific Poly-A selected library preparation followed by 151 bp paired-end sequencing according to the manufacturers protocol (Illumina NovaSeq). Bcl2fastq2 Conversion Software (Illumina) was used to generate de-multiplexed Fastq files. The Fastqreads were trimmed using Cutadapt v2.3.[133] The reads were evaluated with FastQC v0.11.8 to determine quality of the data. Reads were mapped to the reference genome GRCm38 (ENSEMBL), using STAR v2.7.8a[132] and assigned count estimates to genes with RSEM v1.3.3.[131] Alignment options followed ENCODE standards for RNA-seq.[146] QC metrics from several different steps in the pipeline were aggregated by multiQC v1.7.[134] Differential gene expression was performed with DESEQ2. Log2Foldchange (WtvsKO), *p*-value and gene counts were then used in RNA-Enrich[70] software to determine differentially regulated pathways.

Immunoblotting—RIPA buffer (Pierce, cat. #PI89900) supplemented with phosphatase and protease inhibitors (Thermo Scientific cat.# 1862495 and 1862209) was used to lyse cells, and protein concentrations were determined with BCA protein assay (Pierce, cat. #23227). Total protein lysate (10mg) or equivalent cell number lysates were separated by SDS-polyacrylamide gel electrophoresis (Invitrogen) followed by immunoblotting for K48-Ub (CST, cat.# 8081S), XBP1 (Novus Biologicals, cat.# NBP1-77681), ATF4 (CST, cat. #11815S), Sel1L (Abcam, cat. # ab78298), c-MYC (CST, cat. # 5605S), and Beta-actin (Sigma, cat. # A5441-.2ML). Using ImageJ software, bands were quantitated by obtaining mean gray value was for regions of interest encompassing band and lane background was then subtracted. All immunoblots are normalized to beta-actin before normalization to naive or WT.

Immunocytochemistry and confocal microscopy—Fixed cells were incubated in PBST (Phosphate Buffered Saline with 0.1% Triton X-100) containing 2% normal goat serum (Sigma-Aldrich, cat.#G9023) for 30 min at room temperature, followed by labeling with anti-calreticulin (Invitrogen, cat.# PA3-900) diluted 1:50 in PBST. Cells were washed three times with PBST and then incubated in Hoechst diluted 1:1,000 and Alexa Fluor 647 (AF647) goat anti-rabbit (Invitrogen, cat.# A21246) diluted 1:300 in PBST. Labeling steps were carried out at room temperature for 1 h. Cells were then washed, mounted with 90% glycerol diluted with PBS, and imaged by confocal microscopy. Images were acquired with a Leica SP8 confocal scan head mounted to a DMI 6000B CS microscope utilizing a 63X/1.4NA Oil immersion objective. Calreticulin-AF647 and Hoechst images were obtained sequentially by line using 630 nm excitation from a white-light laser paired with a hybrid

detector to acquire calreticulin-AF647 at 662–700 nm, using time gated detection from 0.3 ns–6.0 ns, followed by 405-nm diode laser excitation paired with a separate hybrid detector to detect Hoechst from 415 to 478 nm. Z-stacks were obtained to encompass the majority of the cell volume using a 299 nm step size, where each slice was acquired with a 59 nm pixel size using three-line averages at 400 hz scanning speed recording bi-directionally. All cell stages were imaged during each individual imaging session with the laser power and detector gain held constant during each session. LAS X (ver 3.7.4) was used to export the acquired confocal imaging data into TIF format as well as to generate maximum projections. Pipelines were created in CellProfiler (ver. 4.2.11)[142] to define the overall boundary of individual ER using maximum projections and to measure the total pixel intensity of calreticulin staining (IntegratedIntensity) at individual z-slices within these boundaries. Specifically, to generate the ER outlines using CellProfiler, cells in each maximum projection were first identified by segmenting nuclei into objects from the Hoechst channel using the IdentifyPrimaryObjects module. Global thresholding into three classes was performed using Otsu's method, with middle intensity pixels being assigned to the foreground. A lower bound of 0.05 was used for this thresholding. Clumped objects were both distinguished and divided by shape. Objects touching the edge of an image, as well as objects outside of a diameter range corresponding to a physical size of approximately 3.5–15 μm were discarded by this module. Holes within the identified objects were filled in, after both thresholding and declumping. With these segmented nuclei as seeds, a cell's ER was then segmented from the calreticulin channel with the IdentifySecondaryObjects module using the propagation method with thresholding by Otsu's method. ER objects touching the border of the image were discarded. The resulting ER objects were then saved as binary images that were then loaded into a second pipeline as primary objects via the IdentifyPrimaryObjects module. IntegratedIntensity measurements were then obtained from the calreticulin channel of each slice for each of the ER objects. The z-slice with the greatest IntegratedIntensity for a given cell was used for quantification. Annotated images of the corresponding slices were created by CellProfiler and manually reviewed to exclude any improperly segmented objects from the intensity analysis. To compare calreticulin staining intensities across different imaging sessions, normalized calreticulin staining intensity was calculated for each cell by dividing a given cell's IntegratedIntensity value by the average IntegratedIntensity value of the naive $CD8^+$ T cells acquired during that imaging session.

MERCS microscopy and analysis—T cells were plated in a poly-D-lysine-coated 384-well imaging-grade plates (Phenoplate, PerkinElmer). After adhering by settling, cells were fixed with freshly prepared 4% paraformaldehyde (PFA) at RT for 15 min. Fixed wells were washed with PBS +0.1% Triton X-100 (wash buffer). Wells were blocked with 5% BSA and 10% goat serum in wash buffer (block buffer) for 30 min at RT. A cocktail of anti-KDEL (ab176333; 1:500) and anti-TOM20 (ab56783; 1:500) primary antibodies was prepared in block buffer and incubated in each well for 16 h at 4°C. Wells were washed with wash buffer and stained with AF594-conjugated anti-mouse IgG (A11005; 1:500) and AF488-conjugated anti-rabbit IgG (A11034; 1:500) secondary antibodies and DAPI (4′,6-diamidino-2-phenylindole) (1:1000) counterstain in block buffer for 30 min at RT. Wells were washed with PBS and immediately imaged at 60X magnification on a Cell Voyager 8000 automated confocal microscope (Yokogawa) or

super resolution microscopy via Zeiss LSM 980 with Airyscan 2. During confocal image acquisition, maximum intensity projection (MIP) images were collected across 4 Z-planes spanning 4 μm and centered around a laser autofocus-defined focal plane for each analysis image. Using this automated method >100 cells were sampled per condition for each biological replicate. During Airyscan acquisition, images were collected across 9 Z-planes spanning 1.04 μm. Micrographs were deconvolved with Zeiss Zen software standard deconvolution. 3D rendering of Airyscan micrographs was achieved in Imaris image analysis software using consistent segmentation and surface rendering parameters between conditions. Mitochondria-ER contact sites (MERCS) were defined in Imaris software through thresholding and rendering colocalized regions between the TOM20 and KDEL stain. Representative images shown in this manuscript have uniformly scaled brightness and contrast within each experiment.

Open-source image analysis software CellProfiler was used for quantification of all micrographs. Image analysis was performed on raw images (MIP images from Yokogawa instrument software) using the University of Michigan Advanced Research Computing Great Lakes computing cluster. Automated single-cell analysis was achieved by segmentation of nuclear objects based on nuclear staining, DAPI, using the identify primary objects module, followed by propagation of the nuclear objects to the cellular periphery based on an empirically defined number of pixels roughly equal to the mean nuclear radius using the identify secondary objects module. Mitochondrial objects were defined by segmentation of TOM20 micrographs using two-class Otsu adaptive thresholding of the TOM20 stain in the identify primary objects module. Following object segmentation, the intensity of the KDEL stain in the total cellular and mitochondrial area was measured on a single-cell basis.

Mitochondrial morphology microscopy—At day 3 post activation, ~2–4 × 10^5 cells were seeded on poly-*d*-lysine coverslips and allowed to adhere for 4 hrs at 37°C. Cells were fixed with 4% paraformaldehyde (ThermoFisher, 50980487) for 15 min at 37°C. Coverslips were incubated in blocking solution [5% goat serum (Sigma, G9023) and 0.3% Triton X-100 (Acros Organics, 215682500) in PBS] for 60 min. Coverslips were then incubated in primary antibody solution (1:1,000 Mouse Anti-ATPB (Abcam, ab14730), 1% BSA (Sigma, A9647) and 0.3% Triton X-100 in PBS) at 4°C overnight. After primary incubation, coverslips were washed 3 × in PBS and incubated in secondary antibody solution (1:200 Anti-Mouse Alexa Fluor 488 (Invitrogen, A11029), 1% BSA (Sigma, A9647) and 0.3% Triton X-100 in PBS) for 60 min. Following secondary incubation, coverslips were washed 3 × with PBS and mounted on glass slides using Fluoroshield with DAPI (Sigma, F6057). Triplicate coverslips were used for each biological replicate. Coverslips was imaged using a Zeiss Axio Observer Z1 inverted microscope with LED illumination. Image frames were selected using the DAPI signal to limit bias with 2–5 cells per frame. For each coverslip, 7–8 image z-stacks (0.24 μm slices) capturing the mitochondrial network were acquired at 63 × with oil immersion. Z-stacks were exported as individual image frames in TIFF format for post-processing. Analysis of 3D mitochondrial morphology was adapted from Fogo, Anzell et al.[147] Post-processing was performed in FIJI.[148] The following steps were performed using FIJI's batch processing feature. Background noise was removed using a rolling ball radius of 10 pixels. A median filter was then applied to each image with a radius of 2 pixels.

Mitochondria were segmented using the Trainable Weka Segmentation plug-in.[149] The segmentation classifier model was trained using hand identified ATPB-positive mitochondria from processed images. Segmentation output images were converted to 8-bit binary images and the known scale was set. For the identification of mitochondrial objects in 3D, z-stacks were reconstructed using connected components labeling from the MorphoLibJ plug-in library.[150] Connected stacks were then imported into the 3D object manager,[151] wherein size and shape measurements were acquired. Measures per mitochondrial object were averaged across the 20–24 images (triplicate coverslips) acquired per biological replicate. Image acquisition and post-processing were performed by personnel blinded to condition. 3D mitochondrial morphology was visualized using MeshLab software.[152]

RNA sequencing and analysis—5×10^4 P14 cells per genotype were sorted from mice on day 8 p.i. of LCMV-Armstrong. After sort, cells were washed thoroughly in PBS followed by RNA extraction utilizing the RNA micro kit (Qiagen, cat. #74004) and removing contaminating genomic DNA utilizing DNase I treatment. Library prep and next-generation sequencing was carried out in the Advanced Genomics Core at the University of Michigan. Briefly, RNA was subjected to strand specific Poly-A selected library preparation followed by 151 bp paired-end sequencing according to the manufacturers protocol (Illumina NovaSeq). Bcl2fastq2 Conversion Software (Illumina) was used to generate de-multiplexed Fastq files. The Fastqreads were trimmed using Cutadapt v2.3.[133] The reads were evaluated with FastQC v0.11.8 to determine quality of the data. Reads were mapped to the reference genome GRCm38 (ENSEMBL), using STAR v2.7.8a[132] and assigned count estimates to genes with RSEM v1.3.3.[131] Alignment options followed ENCODE standards for RNA-seq.[146] QC metrics from several different steps in the pipeline were aggregated by multiQC v1.7.[134] Differential gene expression was performed with DESEQ2. Log2Foldchange (WtvsKO), *p*-value and gene counts were then used in RNA-Enrich[70] software to determine differentially regulated pathways.

Bioinformatic re-analysis of public data—For re-analysis of single cell transcriptomics from Kurd et al.,[52] 10x Genomics CellRanger outputs for days 0–7 of LCMV-Armstrong were downloaded from gene expression omnibus GSE131847. Gene UMI tables were processed into scanpy[135] AnnData objects utilizing the scanpy.read_text() function. The dataset was filtered to keep genes identified in at least three cells. Cells containing at less than 200 genes, or more than 5% mitochondrial genes of total genes were removed. Total counts were normalized per cell using the function scanpy.pp.normalize_per_cell(), log transformed sc.pp.log1p(), and scaled scanpy.pp.scale(). scanpy.pl.pca_variance_ratio was used to identify the first eight principal components as meaningful for identifying neighbors scanpy.pp.neighbors() and scanpy.tl.umap(). Single-cell gene set enrichment analysis was conducted utilizing the python implementation of decoupleR.[136] Gene Matrix file corresponding to murine Gene ontologies m5.go.v2023.1.Mm.symbols was downloaded from MSigDB.[153] Decoupler.run_ORA() was used to generate pathway enrichment statistics. Data was exported and visualized using ggplot2 in R.

For analysis of Rieckmann et al.,[93] processed and quantified data were downloaded from ProteomeXchange partner PRIDE (PXD004352) in Maxquant output format. Label free quantification of protein from "MaxLFQ" was then used for differential protein expression analysis.[154] Proteomes of $CD8^+$ T cell subsets at different activation states were then used to identify differentially expressed protein with parametric one-way ANOVA with Dunnett's multiple comparisons post-hoc test.

For Giles et al.[92] and Weber et al.,[100] raw reads were downloaded from the Sequencing Read Archive (PRJNA744266, PRJNA692497) utilizing the SRATools fastqdump command. Data was processed using nf-core/rnaseq v3.12.0 (doi: https://doi.org/10.5281/zenodo.1400710) of the nf-core collection of workflows.[141] Briefly, FASTQC was used to assess sequence quality. STAR[132] was used to align reads to reference transcriptome hg38. RSEM[131] was then used to estimate gene and isoform expression levels. RSEM counts were then imported into DESEQ2[129] for differential expression analysis. For Giles et al.,[92] only data corresponding to $CD8^+$ T cells was processed. Gene Set Variation analysis was conducted utilizing GSVA R package[137] with Human biological pathways gene ontologies C5 and Hallmarks H. Turkeys' multiple comparison test was used to determine the significance in gene set score between $CD8^+$ T cell subsets. For Weber et al.,[100] data was processed as above. DESEQ2 was used to identify differential expression between genes at day 15 undergoing continuous stimulation versus transiently rested cells. FGSEA[139] was used to perform gene set enrichment analysis using msigdb gene sets for gene ontology (C5) and hallmark (H). For Phillipp et al.,[99] raw counts were downloaded from GSE196463 and loaded into DESEQ2, and FGSEA was used as above.

QUANTIFICATION AND STATISTICAL ANALYSIS

No statistical methods were used to predetermine sample size. Statistical tests used for each experiment are detailed in the figure legends and were calculated using Prism (version 10). Number (n) represents biological replicate, i.e., individual mouse or human. Error bars indicate standard deviation unless otherwise specified. To test for normality the following test were conducted Anderson-Darlin, Shapiro-Wilk, Kolmogorov-Smirnov as well as inspection of quantile quartile plots. Data corresponding to the co-transfer experiment in which WT and KO cells are in the same mouse, or the paired comparison of the same human T cells under different parallel conditions, paired two-tailed t test were conducted. For statistical analysis of three or more normally distributed groups, one-way ANOVA was used, followed by Fisher's least significant difference to determine multiple comparisons. Comparisons of three or more groups that are normally distributed to a control group were conducted using one-way ANOVA followed by Dunnett's multiple comparison test. In comparisons of data with three or more groups that are sequentially tracked and are not normally distributed, Friedman's test with uncorrected Dunnett's multiple comparison test was used. For comparison of three or more groups that were not sequentially tracked and are not normally distributed, the Kruskal-Wallis test was conducted with follow-up for multiple comparisons to a control group by Dunnett's multiple comparison test.

Supplementary Material

Refer to Web version on PubMed Central for supplementary material.

ACKNOWLEDGMENTS

We thank Richard Lee of the University of Michigan for calreticulin confocal imaging and Dr. Jonathan Sexton for use of the automated microscope for quantitative imaging of ER and mitochondria. We also thank Dr. Ling Qi of the University of Virginia for the Sel1L mice. We thank members of the Carty and Moore labs for helpful discussions. This work was funded through the National Institutes of Health by R01 AI165533 (S.A.C.), T32 AI007413 (L.O.C.-M., H.S.H., N.D.A., M.B.R., and D.A.), T32 CA140044 (L.O.C.-M.), F99 AG079793 (G.M.F.), R01 AI157384 (M.X.O.), R01 NS120322 (T.H.S.), R01 AI157384 (M.X.O.), Miller Fund for Innovative Immunology Research (L.O.C.-M. and M.B.R.), University of Michigan Rogel Cancer Center (S.A.C.), Limpert Clinical Scholar Award (S.A.C.), Elsa U. Pardee Foundation (S.A.C.), and American Heart Association 23PRE1019508 (M.B.R.). L.O.C.-M. was also supported by a Rackham Predoctoral Fellowship from the University of Michigan and American Association of Immunologists' Careers in Immunology fellowship. We acknowledge support from the University of Michigan Biomedical Research Core Facilities (Microscopy and Flow Cytometry cores). Further support was provided by the National Cancer Institute of the National Institutes of Health (P30CA046592) by the use of the following Cancer Center Shared Resources: Flow Cytometry. We thank the NIH Tetramer Core Facility (contract number 75N93020D00005) for providing gp33 and NP396 tetramers.

REFERENCES

1. Wong P, and Pamer EG (2003). CD8 T cell responses to infectious pathogens. Annu. Rev. Immunol. 21, 29–70. 10.1146/annurev.immunol.21.120601.141114. [PubMed: 12414723]
2. Murali-Krishna K, Altman JD, Suresh M, Sourdive DJ, Zajac AJ, Miller JD, Slansky J, and Ahmed R (1998). Counting antigen-specific CD8 T cells: a reevaluation of bystander activation during viral infection. Immunity 8, 177–187. 10.1016/s1074-7613(00)80470-7. [PubMed: 9491999]
3. Philip M, and Schietinger A (2022). CD8(+) T cell differentiation and dysfunction in cancer. Nat. Rev. Immunol. 22, 209–223. 10.1038/s41577-021-00574-3. [PubMed: 34253904]
4. Jameson SC, and Masopust D (2018). Understanding Subset Diversity in T Cell Memory. Immunity 48, 214–226. 10.1016/j.immuni.2018.02.010. [PubMed: 29466754]
5. Badovinac VP, Porter BB, and Harty JT (2002). Programmed contraction of CD8(+) T cells after infection. Nat. Immunol. 3, 619–626. 10.1038/ni804. [PubMed: 12055624]
6. Marchingo JM, and Cantrell DA (2022). Protein synthesis, degradation, and energy metabolism in T cell immunity. Cell. Mol. Immunol. 19, 303–315. 10.1038/s41423-021-00792-8. [PubMed: 34983947]
7. Gray SM, Kaech SM, and Staron MM (2014). The interface between transcriptional and epigenetic control of effector and memory CD8(+) T-cell differentiation. Immunol. Rev. 261, 157–168. 10.1111/imr.12205. [PubMed: 25123283]
8. Reina-Campos M, Scharping NE, and Goldrath AW (2021). CD8(+) T cell metabolism in infection and cancer. Nat. Rev. Immunol. 21, 718–738. 10.1038/s41577-021-00537-8. [PubMed: 33981085]
9. Araki K, Morita M, Bederman AG, Konieczny BT, Kissick HT, Sonenberg N, and Ahmed R (2017). Translation is actively regulated during the differentiation of CD8(+) effector T cells. Nat. Immunol. 18, 1046–1057. 10.1038/ni.3795. [PubMed: 28714979]
10. Wolf T, Jin W, Zoppi G, Vogel IA, Akhmedov M, Bleck CKE, Beltraminelli T, Rieckmann JC, Ramirez NJ, Benevento M, et al. (2020). Dynamics in protein translation sustaining T cell preparedness. Nat. Immunol. 21, 927–937. 10.1038/s41590-020-0714-5. [PubMed: 32632289]
11. Howden AJM, Hukelmann JL, Brenes A, Spinelli L, Sinclair LV, Lamond AI, and Cantrell DA (2019). Quantitative analysis of T cell proteomes and environmental sensors during T cell differentiation. Nat. Immunol. 20, 1542–1554. 10.1038/s41590-019-0495-x. [PubMed: 31591570]
12. Marchingo JM, Sinclair LV, Howden AJ, and Cantrell DA (2020). Quantitative analysis of how Myc controls T cell proteomes and metabolic pathways during T cell activation. Elife 9, e53725. 10.7554/eLife.53725. [PubMed: 32022686]

13. Damasio MP, Marchingo JM, Spinelli L, Hukelmann JL, Cantrell DA, and Howden AJM (2021). Extracellular signal-regulated kinase (ERK) pathway control of CD8+ T cell differentiation. Biochem. J. 478, 79–98. 10.1042/BCJ20200661. [PubMed: 33305809]

14. Ron-Harel N, Santos D, Ghergurovich JM, Sage PT, Reddy A, Lovitch SB, Dephoure N, Satterstrom FK, Sheffer M, Spinelli JB, et al. (2016). Mitochondrial Biogenesis and Proteome Remodeling Promote One-Carbon Metabolism for T Cell Activation. Cell Metab. 24, 104–117. 10.1016/j.cmet.2016.06.007. [PubMed: 27411012]

15. Tan H, Yang K, Li Y, Shaw TI, Wang Y, Blanco DB, Wang X, Cho JH, Wang H, Rankin S, et al. (2017). Integrative Proteomics and Phosphoproteomics Profiling Reveals Dynamic Signaling Networks and Bioenergetics Pathways Underlying T Cell Activation. Immunity 46, 488–503. 10.1016/j.immuni.2017.02.010. [PubMed: 28285833]

16. Schubert U, Antón LC, Gibbs J, Norbury CC, Yewdell JW, and Bennink JR (2000). Rapid degradation of a large fraction of newly synthesized proteins by proteasomes. Nature 404, 770–774. 10.1038/35008096. [PubMed: 10783891]

17. Lykke-Andersen J, and Bennett EJ (2014). Protecting the proteome: Eukaryotic cotranslational quality control pathways. J. Cell Biol. 204, 467–476. 10.1083/jcb.201311103. [PubMed: 24535822]

18. Walter P, and Ron D (2011). The unfolded protein response: from stress pathway to homeostatic regulation. Science 334, 1081–1086. 10.1126/science.1209038. [PubMed: 22116877]

19. Hetz C (2012). The unfolded protein response: controlling cell fate decisions under ER stress and beyond. Nat. Rev. Mol. Cell Biol. 13, 89–102. 10.1038/nrm3270. [PubMed: 22251901]

20. Widjaja CE, Olvera JG, Metz PJ, Phan AT, Savas JN, de Bruin G, Leestemaker Y, Berkers CR, de Jong A, Florea BI, et al. (2017). Proteasome activity regulates CD8+ T lymphocyte metabolism and fate specification. J. Clin. Invest. 127, 3609–3623. 10.1172/JCI90895. [PubMed: 28846070]

21. Ma X, Bi E, Lu Y, Su P, Huang C, Liu L, Wang Q, Yang M, Kalady MF, Qian J, et al. (2019). Cholesterol Induces CD8(+) T Cell Exhaustion in the Tumor Microenvironment. Cell Metab. 30, 143–156.e5. 10.1016/j.cmet.2019.04.002. [PubMed: 31031094]

22. Kamimura D, and Bevan MJ (2008). Endoplasmic reticulum stress regulator XBP-1 contributes to effector CD8+ T cell differentiation during acute infection. J. Immunol. 181, 5433–5441. 10.4049/jimmunol.181.8.5433. [PubMed: 18832700]

23. Cao Y, Trillo-Tinoco J, Sierra RA, Anadon C, Dai W, Mohamed E, Cen L, Costich TL, Magliocco A, Marchion D, et al. (2019). ER stress-induced mediator C/EBP homologous protein thwarts effector T cell activity in tumors through T-bet repression. Nat. Commun. 10, 1280. 10.1038/s41467-019-09263-1. [PubMed: 30894532]

24. Mueller B, Lilley BN, and Ploegh HL (2006). SEL1L, the homologue of yeast Hrd3p, is involved in protein dislocation from the mammalian ER. J. Cell Biol. 175, 261–270. 10.1083/jcb.200605196. [PubMed: 17043138]

25. Sun S, Shi G, Han X, Francisco AB, Ji Y, Mendonc a, N., Liu X, Locasale JW, Simpson KW, Duhamel GE, et al. (2014). Sel1L is indispensable for mammalian endoplasmic reticulum-associated degradation, endoplasmic reticulum homeostasis, and survival. Proc. Natl. Acad. Sci. USA 111, E582–E591. 10.1073/pnas.1318114111. [PubMed: 24453213]

26. Shrestha N, Liu T, Ji Y, Reinert RB, Torres M, Li X, Zhang M, Tang CHA, Hu CCA, Liu C, et al. (2020). Sel1L-Hrd1 ER-associated degradation maintains beta cell identity via TGF-beta signaling. J. Clin. Invest. 130, 3499–3510. 10.1172/JCI134874. [PubMed: 32182217]

27. Ji Y, Kim H, Yang L, Sha H, Roman CA, Long Q, and Qi L (2016). The Sel1L-Hrd1 Endoplasmic Reticulum-Associated Degradation Complex Manages a Key Checkpoint in B Cell Development. Cell Rep. 16, 2630–2640. 10.1016/j.celrep.2016.08.003. [PubMed: 27568564]

28. Xu L, Liu X, Peng F, Zhang W, Zheng L, Ding Y, Gu T, Lv K, Wang J, Ortinau L, et al. (2020). Protein quality control through endoplasmic reticulum-associated degradation maintains haematopoietic stem cell identity and niche interactions. Nat. Cell Biol. 22, 1162–1169. 10.1038/s41556-020-00581-x. [PubMed: 32958856]

29. Liu X, Yu J, Xu L, Umphred-Wilson K, Peng F, Ding Y, Barton BM, Lv X, Zhao MY, Sun S, et al. (2021). Notch-induced endoplasmic reticulum-associated degradation governs mouse thymocyte beta-selection. Elife 10, e69975. 10.7554/eLife.69975. [PubMed: 34240701]

30. Thepsuwan P, Bhattacharya A, Song Z, Hippleheuser S, Feng S, Wei X, Das NK, Sierra M, Wei J, Fang D, et al. (2023). Hepatic SEL1L-HRD1 ER-associated degradation regulates systemic iron homeostasis via ceruloplasmin. Proc. Natl. Acad. Sci. USA 120, e2212644120. 10.1073/pnas.2212644120. [PubMed: 36595688]

31. Bhattacharya A, Sun S, Wang H, Liu M, Long Q, Yin L, Kersten S, Zhang K, and Qi L (2018). Hepatic Sel1L-Hrd1 ER-associated degradation (ERAD) manages FGF21 levels and systemic metabolism via CREBH. EMBO J. 37, e99277. 10.15252/embj.201899277. [PubMed: 30389665]

32. Sha H, Sun S, Francisco AB, Ehrhardt N, Xue Z, Liu L, Lawrence P, Mattijssen F, Guber RD, Panhwar MS, et al. (2014). The ER-associated degradation adaptor protein Sel1L regulates LPL secretion and lipid metabolism. Cell Metab. 20, 458–470. 10.1016/j.cmet.2014.06.015. [PubMed: 25066055]

33. Sun S, Lourie R, Cohen SB, Ji Y, Goodrich JK, Poole AC, Ley RE, Denkers EY, McGuckin MA, Long Q, et al. (2016). Epithelial Sel1L is required for the maintenance of intestinal homeostasis. Mol. Biol. Cell 27, 483–490. 10.1091/mbc.E15-10-0724. [PubMed: 26631554]

34. Zhou Z, Torres M, Sha H, Halbrook CJ, Van den Bergh F, Reinert RB, Yamada T, Wang S, Luo Y, Hunter AH, et al. (2020). Endoplasmic reticulum-associated degradation regulates mitochondrial dynamics in brown adipocytes. Science 368, 54–60. 10.1126/science.aay2494. [PubMed: 32193362]

35. Yoshida S, Wei X, Zhang G, O'Connor CL, Torres M, Zhou Z, Lin L, Menon R, Xu X, Zheng W, et al. (2021). Endoplasmic reticulum-associated degradation is required for nephrin maturation and kidney glomerular filtration function. J. Clin. Invest. 131, e143988. 10.1172/JCI143988. [PubMed: 33591954]

36. Wei J, Yuan Y, Chen L, Xu Y, Zhang Y, Wang Y, Yang Y, Peek CB, Diebold L, Yang Y, et al. (2018). ER-associated ubiquitin ligase HRD1 programs liver metabolism by targeting multiple metabolic enzymes. Nat. Commun. 9, 3659. 10.1038/s41467-018-06091-7. [PubMed: 30201971]

37. Xu Y, Melo-Cardenas J, Zhang Y, Gau I, Wei J, Montauti E, Zhang Y, Gao B, Jin H, Sun Z, et al. (2019). The E3 ligase Hrd1 stabilizes Tregs by antagonizing inflammatory cytokine-induced ER stress response. JCI Insight 4, e121887. 10.1172/jci.insight.121887. [PubMed: 30843874]

38. Dils AT, Correa LO, Gronevelt JP, Liu L, Kadiyala P, Li Q, and Carty SA (2021). The Endoplasmic Reticulum Associated Degradation Adaptor Sel1L Regulates T Cell Homeostasis and Function. Preprint at bioRxiv. 10.1101/2021.05.22.445275.

39. Gao Y, Li W, Wang Z, Zhang C, He Y, Liu X, Tang K, Zhang W, Long Q, Liu Y, et al. (2023). SEL1L preserves CD8(+) T-cell survival and homeostasis by fine-tuning PERK signaling and the IL-15 receptor-mediated mTORC1 axis. Cell. Mol. Immunol. 20, 1232–1250. 10.1038/s41423-023-01078-x. [PubMed: 37644166]

40. Rollings CM, Sinclair LV, Brady HJM, Cantrell DA, and Ross SH (2018). Interleukin-2 shapes the cytotoxic T cell proteome and immune environment-sensing programs. Sci. Signal. 11, eaap8112. 10.1126/scisignal.aap8112. [PubMed: 29666307]

41. Carrio R, Bathe OF, and Malek TR (2004). Initial antigen encounter programs CD8+ T cells competent to develop into memory cells that are activated in an antigen-free, IL-7- and IL-15-rich environment. J. Immunol. 172, 7315–7323. 10.4049/jimmunol.172.12.7315. [PubMed: 15187107]

42. van der Windt GJW, Everts B, Chang CH, Curtis JD, Freitas TC, Amiel E, Pearce EJ, and Pearce EL (2012). Mitochondrial respiratory capacity is a critical regulator of CD8+ T cell memory development. Immunity 36, 68–78. 10.1016/j.immuni.2011.12.007. [PubMed: 22206904]

43. Schuck S, Prinz WA, Thorn KS, Voss C, and Walter P (2009). Membrane expansion alleviates endoplasmic reticulum stress independently of the unfolded protein response. J. Cell Biol. 187, 525–536. 10.1083/jcb.200907074. [PubMed: 19948500]

44. Bernales S, McDonald KL, and Walter P (2006). Autophagy counter-balances endoplasmic reticulum expansion during the unfolded protein response. PLoS Biol. 4, e423. 10.1371/journal.pbio.0040423. [PubMed: 17132049]

45. Williams DB (2006). Beyond lectins: the calnexin/calreticulin chaperone system of the endoplasmic reticulum. J. Cell Sci. 119, 615–623. 10.1242/jcs.02856. [PubMed: 16467570]

46. Kim S, Khoriaty R, Li L, McClune M, Kalfa TA, Wu J, Peltier D, Fujiwara H, Sun Y, Oravecz-Wilson K, et al. (2021). ER-to-Golgi transport and SEC23-dependent COPII vesicles regulate T cell alloimmunity. J. Clin. Invest. 131, e136574. 10.1172/JCI136574. [PubMed: 33463537]
47. Johnston JA, Ward CL, and Kopito RR (1998). Aggresomes: a cellular response to misfolded proteins. J. Cell Biol. 143, 1883–1898. 10.1083/jcb.143.7.1883. [PubMed: 9864362]
48. Chau V, Tobias JW, Bachmair A, Marriott D, Ecker DJ, Gonda DK, and Varshavsky A (1989). A multiubiquitin chain is confined to specific lysine in a targeted short-lived protein. Science 243, 1576–1583. 10.1126/science.2538923. [PubMed: 2538923]
49. Yoshida H, Matsui T, Yamamoto A, Okada T, and Mori K (2001). XBP1 mRNA is induced by ATF6 and spliced by IRE1 in response to ER stress to produce a highly active transcription factor. Cell 107, 881–891. 10.1016/s0092-8674(01)00611-0. [PubMed: 11779464]
50. Calfon M, Zeng H, Urano F, Till JH, Hubbard SR, Harding HP, Clark SG, and Ron D (2002). IRE1 couples endoplasmic reticulum load to secretory capacity by processing the XBP-1 mRNA. Nature 415, 92–96. 10.1038/415092a. [PubMed: 11780124]
51. Hurst KE, Lawrence KA, Essman MT, Walton ZJ, Leddy LR, and Thaxton JE (2019). Endoplasmic Reticulum Stress Contributes to Mitochondrial Exhaustion of CD8(+) T Cells. Cancer Immunol. Res. 7, 476–486. 10.1158/2326-6066.CIR-18-0182. [PubMed: 30659052]
52. Kurd NS, He Z, Louis TL, Milner JJ, Omilusik KD, Jin W, Tsai MS, Widjaja CE, Kanbar JN, Olvera JG, et al. (2020). Early precursors and molecular determinants of tissue-resident memory CD8(+) T lymphocytes revealed by single-cell RNA sequencing. Sci. Immunol. 5, eaaz6894. 10.1126/sciimmunol.aaz6894. [PubMed: 32414833]
53. Blazanin N, Son J, Craig-Lucas AB, John CL, Breech KJ, Podol-sky MA, and Glick AB (2017). ER stress and distinct outputs of the IRE1alpha RNase control proliferation and senescence in response to oncogenic Ras. Proc. Natl. Acad. Sci. USA 114, 9900–9905. 10.1073/pnas.1701757114. [PubMed: 28847931]
54. Song M, Sandoval TA, Chae CS, Chopra S, Tan C, Rutkowski MR, Raundhal M, Chaurio RA, Payne KK, Konrad C, et al. (2018). IRE1alpha-XBP1 controls T cell function in ovarian cancer by regulating mitochondrial activity. Nature 562, 423–428. 10.1038/s41586-018-0597-x. [PubMed: 30305738]
55. Riesenberg BP, Hunt EG, Tennant MD, Hurst KE, Andrews AM, Leddy LR, Neskey DM, Hill EG, Rivera GOR, Paulos CM, et al. (2022). Stress-Mediated Attenuation of Translation Undermines T-cell Activity in Cancer. Cancer Res. 82, 4386–4399. 10.1158/0008-5472.CAN-22-1744. [PubMed: 36126165]
56. Li S, Francisco AB, Munroe RJ, Schimenti JC, and Long Q (2010). SEL1L deficiency impairs growth and differentiation of pancreatic epithelial cells. BMC Dev. Biol. 10, 19. 10.1186/1471-213X-10-19. [PubMed: 20170518]
57. McCausland MM, and Crotty S (2008). Quantitative PCR technique for detecting lymphocytic choriomeningitis virus in vivo. J. Virol. Methods 147, 167–176. 10.1016/j.jviromet.2007.08.025. [PubMed: 17920702]
58. Akondy RS, Monson ND, Miller JD, Edupuganti S, Teuwen D, Wu H, Quyyumi F, Garg S, Altman JD, Del Rio C, et al. (2009). The yellow fever virus vaccine induces a broad and polyfunctional human memory CD8+ T cell response. J. Immunol. 183, 7919–7930. 10.4049/jimmunol.0803903. [PubMed: 19933869]
59. Betts MR, Nason MC, West SM, De Rosa SC, Migueles SA, Abraham J, Lederman MM, Benito JM, Goepfert PA, Connors M, et al. (2006). HIV nonprogressors preferentially maintain highly functional HIV-specific CD8+ T cells. Blood 107, 4781–4789. 10.1182/blood-2005-12-4818. [PubMed: 16467198]
60. Roederer M, Nozzi JL, and Nason MC (2011). SPICE: exploration and analysis of post-cytometric complex multivariate datasets. Cytometry A. 79, 167–174. 10.1002/cyto.a.21015. [PubMed: 21265010]
61. Joshi NS, Cui W, Chandele A, Lee HK, Urso DR, Hagman J, Gapin L, and Kaech SM (2007). Inflammation directs memory precursor and short-lived effector CD8(+) T cell fates via the graded expression of T-bet transcription factor. Immunity 27, 281–295. 10.1016/j.immuni.2007.07.010. [PubMed: 17723218]

62. Kaech SM, Tan JT, Wherry EJ, Konieczny BT, Surh CD, and Ahmed R (2003). Selective expression of the interleukin 7 receptor identifies effector CD8 T cells that give rise to long-lived memory cells. Nat. Immunol. 4, 1191–1198. 10.1038/ni1009. [PubMed: 14625547]

63. Sarkar S, Kalia V, Haining WN, Konieczny BT, Subramaniam S, and Ahmed R (2008). Functional and genomic profiling of effector CD8 T cell subsets with distinct memory fates. J. Exp. Med. 205, 625–640. 10.1084/jem.20071641. [PubMed: 18316415]

64. Jeannet G, Boudousquié C, Gardiol N, Kang J, Huelsken J, and Held W (2010). Essential role of the Wnt pathway effector Tcf-1 for the establishment of functional CD8 T cell memory. Proc. Natl. Acad. Sci. USA 107, 9777–9782. 10.1073/pnas.0914127107. [PubMed: 20457902]

65. Zhou X, Yu S, Zhao DM, Harty JT, Badovinac VP, and Xue HH (2010). Differentiation and persistence of memory CD8(+) T cells depend on T cell factor 1. Immunity 33, 229–240. 10.1016/j.immuni.2010.08.002. [PubMed: 20727791]

66. Zhou X, and Xue HH (2012). Cutting edge: generation of memory precursors and functional memory CD8+ T cells depends on T cell factor-1 and lymphoid enhancer-binding factor-1. J. Immunol. 189, 2722–2726. 10.4049/jimmunol.1201150. [PubMed: 22875805]

67. Sallusto F, Lenig D, Förster R, Lipp M, and Lanzavecchia A (1999). Two subsets of memory T lymphocytes with distinct homing potentials and effector functions. Nature 401, 708–712. 10.1038/44385. [PubMed: 10537110]

68. Wherry EJ, Teichgräber V, Becker TC, Masopust D, Kaech SM, Antia R, von Andrian UH, and Ahmed R (2003). Lineage relationship and protective immunity of memory CD8 T cell subsets. Nat. Immunol. 4, 225–234. 10.1038/ni889. [PubMed: 12563257]

69. Hikono H, Kohlmeier JE, Takamura S, Wittmer ST, Roberts AD, and Woodland DL (2007). Activation phenotype, rather than central-or effector-memory phenotype, predicts the recall efficacy of memory CD8+ T cells. J. Exp. Med. 204, 1625–1636. 10.1084/jem.20070322. [PubMed: 17606632]

70. Lee C, Patil S, and Sartor MA (2016). RNA-Enrich: a cut-off free functional enrichment testing method for RNA-seq with improved detection power. Bioinformatics 32, 1100–1102. 10.1093/bioinformatics/btv694. [PubMed: 26607492]

71. Han J, Back SH, Hur J, Lin YH, Gildersleeve R, Shan J, Yuan CL, Krokowski D, Wang S, Hatzoglou M, et al. (2013). ER-stress-induced transcriptional regulation increases protein synthesis leading to cell death. Nat. Cell Biol. 15, 481–490. 10.1038/ncb2738. [PubMed: 23624402]

72. Mishra P, Carelli V, Manfredi G, and Chan DC (2014). Proteolytic cleavage of Opa1 stimulates mitochondrial inner membrane fusion and couples fusion to oxidative phosphorylation. Cell Metab. 19, 630–641. 10.1016/j.cmet.2014.03.011. [PubMed: 24703695]

73. Cogliati S, Frezza C, Soriano ME, Varanita T, Quintana-Cabrera R, Corrado M, Cipolat S, Costa V, Casarin A, Gomes LC, et al. (2013). Mitochondrial cristae shape determines respiratory chain supercomplexes assembly and respiratory efficiency. Cell 155, 160–171. 10.1016/j.cell.2013.08.032. [PubMed: 24055366]

74. Buck MD, O'Sullivan D, Klein Geltink RI, Curtis JD, Chang CH, Sanin DE, Qiu J, Kretz O, Braas D, van der Windt GJW, et al. (2016). Mitochondrial Dynamics Controls T Cell Fate through Metabolic Programming. Cell 166, 63–76. 10.1016/j.cell.2016.05.035. [PubMed: 27293185]

75. Hunt EG, Andrews AM, Larsen SR, and Thaxton JE (2022). The ER-Mitochondria Interface as a Dynamic Hub for T Cell Efficacy in Solid Tumors. Front. Cell Dev. Biol. 10, 867341. 10.3389/fcell.2022.867341. [PubMed: 35573704]

76. Rowland AA, and Voeltz GK (2012). Endoplasmic reticulum-mitochondria contacts: function of the junction. Nat. Rev. Mol. Cell Biol. 13, 607–625. 10.1038/nrm3440. [PubMed: 22992592]

77. Baixauli F, Piletic K, Puleston DJ, Villa M, Field CS, Flachsmann LJ, Quintana A, Rana N, Edwards-Hicks J, Matsushita M, et al. (2022). An LKB1-mitochondria axis controls T(H)17 effector function. Nature 610, 555–561. 10.1038/s41586-022-05264-1. [PubMed: 36171294]

78. Stevens MG, Mason FM, and Bullock TNJ (2024). The mitochondrial fission protein DRP1 influences memory CD8+ T cell formation and function. J. Leukoc. Biol. 115, 679–694. 10.1093/jleuko/qiad155. [PubMed: 38057151]

79. Wang R, Dillon CP, Shi LZ, Milasta S, Carter R, Finkelstein D, McCormick LL, Fitzgerald P, Chi H, Munger J, and Green DR (2011). The transcription factor Myc controls metabolic reprogramming upon T lymphocyte activation. Immunity 35, 871–882. 10.1016/j.immuni.2011.09.021. [PubMed: 22195744]
80. Preston GC, Sinclair LV, Kaskar A, Hukelmann JL, Navarro MN, Ferrero I, MacDonald HR, Cowling VH, and Cantrell DA (2015). Single cell tuning of Myc expression by antigen receptor signal strength and interleukin-2 in T lymphocytes. EMBO J. 34, 2008–2024. 10.15252/embj.201490252. [PubMed: 26136212]
81. Chan JD, Lai J, Slaney CY, Kallies A, Beavis PA, and Darcy PK (2021). Cellular networks controlling T cell persistence in adoptive cell therapy. Nat. Rev. Immunol. 21, 769–784. 10.1038/s41577-021-00539-6. [PubMed: 33879873]
82. Cui W, and Kaech SM (2010). Generation of effector CD8+ T cells and their conversion to memory T cells. Immunol. Rev. 236, 151–166. 10.1111/j.1600-065X.2010.00926.x. [PubMed: 20636815]
83. Akondy RS, Fitch M, Edupuganti S, Yang S, Kissick HT, Li KW, Youngblood BA, Abdelsamed HA, McGuire DJ, Cohen KW, et al. (2017). Origin and differentiation of human memory CD8 T cells after vaccination. Nature 552, 362–367. 10.1038/nature24633. [PubMed: 29236685]
84. Fraietta JA, Nobles CL, Sammons MA, Lundh S, Carty SA, Reich TJ, Cogdill AP, Morrissette JJD, DeNizio JE, Reddy S, et al. (2018). Disruption of TET2 promotes the therapeutic efficacy of CD19-targeted T cells. Nature 558, 307–312. 10.1038/s41586-018-0178-z. [PubMed: 29849141]
85. Restifo NP, and Gattinoni L (2013). Lineage relationship of effector and memory T cells. Curr. Opin. Immunol. 25, 556–563. 10.1016/j.coi.2013.09.003. [PubMed: 24148236]
86. Fuertes Marraco SA, Soneson C, Cagnon L, Gannon PO, Allard M, Maillard SA, Montandon N, Rufer N, Waldvogel S, Delorenzi M, and Speiser DE (2015). Long-lasting stem cell-like memory CD8+ T cells with a naive-like profile upon yellow fever vaccination. Sci. Transl. Med. 7, 282ra248. 10.1126/scitranslmed.aaa3700.
87. Gattinoni L, Lugli E, Ji Y, Pos Z, Paulos CM, Quigley MF, Almeida JR, Gostick E, Yu Z, Carpenito C, et al. (2011). A human memory T cell subset with stem cell-like properties. Nat. Med. 17, 1290–1297. 10.1038/nm.2446. [PubMed: 21926977]
88. Willinger T, Freeman T, Herbert M, Hasegawa H, McMichael AJ, and Callan MFC (2006). Human naive CD8 T cells down-regulate expression of the WNT pathway transcription factors lymphoid enhancer binding factor 1 and transcription factor 7 (T cell factor-1) following antigen encounter in vitro and in vivo. J. Immunol. 176, 1439–1446. 10.4049/jimmunol.176.3.1439. [PubMed: 16424171]
89. Pauken KE, Sammons MA, Odorizzi PM, Manne S, Godec J, Khan O, Drake AM, Chen Z, Sen DR, Kurachi M, et al. (2016). Epigenetic stability of exhausted T cells limits durability of reinvigoration by PD-1 blockade. Science 354, 1160–1165. 10.1126/science.aaf2807. [PubMed: 27789795]
90. Chen Z, Ji Z, Ngiow SF, Manne S, Cai Z, Huang AC, Johnson J, Staupe RP, Bengsch B, Xu C, et al. (2019). TCF-1-Centered Transcriptional Network Drives an Effector versus Exhausted CD8 T Cell-Fate Decision. Immunity 51, 840–855.e5. 10.1016/j.immuni.2019.09.013. [PubMed: 31606264]
91. Yao C, Sun HW, Lacey NE, Ji Y, Moseman EA, Shih HY, Heuston EF, Kirby M, Anderson S, Cheng J, et al. (2019). Single-cell RNA-seq reveals TOX as a key regulator of CD8(+) T cell persistence in chronic infection. Nat. Immunol. 20, 890–901. 10.1038/s41590-019-0403-4. [PubMed: 31209400]
92. Giles JR, Manne S, Freilich E, Oldridge DA, Baxter AE, George S, Chen Z, Huang H, Chilukuri L, Carberry M, et al. (2022). Human epigenetic and transcriptional T cell differentiation atlas for identifying functional T cell-specific enhancers. Immunity 55, 557–574.e7. 10.1016/j.immuni.2022.02.004. [PubMed: 35263570]
93. Rieckmann JC, Geiger R, Hornburg D, Wolf T, Kveler K, Jarrossay D, Sallusto F, Shen-Orr SS, Lanzavecchia A, Mann M, and Meissner F (2017). Social network architecture of human immune cells unveiled by quantitative proteomics. Nat. Immunol. 18, 583–593. 10.1038/ni.3693. [PubMed: 28263321]

94. Yamamoto K, Suzuki N, Wada T, Okada T, Yoshida H, Kaufman RJ, and Mori K (2008). Human HRD1 promoter carries a functional unfolded protein response element to which XBP1 but not ATF6 directly binds. J. Biochem. 144, 477–486. 10.1093/jb/mvn091. [PubMed: 18664523]

95. Yoshida H, Matsui T, Hosokawa N, Kaufman RJ, Nagata K, and Mori K (2003). A time-dependent phase shift in the mammalian unfolded protein response. Dev. Cell 4, 265–271. 10.1016/s1534-5807(03)00022-4. [PubMed: 12586069]

96. Lee AH, Iwakoshi NN, and Glimcher LH (2003). XBP-1 regulates a subset of endoplasmic reticulum resident chaperone genes in the unfolded protein response. Mol. Cell Biol. 23, 7448–7459. 10.1128/MCB.23.21.7448-7459.2003. [PubMed: 14559994]

97. June CH, O'Connor RS, Kawalekar OU, Ghassemi S, and Milone MC (2018). CAR T cell immunotherapy for human cancer. Science 359, 1361–1365. 10.1126/science.aar6711. [PubMed: 29567707]

98. Goebeler ME, and Bargou RC (2020). T cell-engaging therapies - BiTEs and beyond. Nat. Rev. Clin. Oncol. 17, 418–434. 10.1038/s41571-020-0347-5. [PubMed: 32242094]

99. Philipp N, Kazerani M, Nicholls A, Vick B, Wulf J, Straub T, Scheurer M, Muth A, Hänel G, Nixdorf D, et al. (2022). T-cell exhaustion induced by continuous bispecific molecule exposure is ameliorated by treatment-free intervals. Blood 140, 1104–1118. 10.1182/blood.2022015956. [PubMed: 35878001]

100. Weber EW, Parker KR, Sotillo E, Lynn RC, Anbunathan H, Lattin J, Good Z, Belk JA, Daniel B, Klysz D, et al. (2021). Transient rest restores functionality in exhausted CAR-T cells through epigenetic remodeling. Science 372, eaba1786. 10.1126/science.aba1786. [PubMed: 33795428]

101. Soares Moretti AI, and Martins Laurindo FR (2017). Protein disulfide isomerases: Redox connections in and out of the endoplasmic reticulum. Arch. Biochem. Biophys. 617, 106–119. 10.1016/j.abb.2016.11.007. [PubMed: 27889386]

102. Hurst KE, Lawrence KA, Reyes Angeles L, Ye Z, Zhang J, Town-send DM, Dolloff N, and Thaxton JE (2019). Endoplasmic Reticulum Protein Disulfide Isomerase Shapes T Cell Efficacy for Adoptive Cellular Therapy of Tumors. Cells 8, 1514. 10.3390/cells8121514. [PubMed: 31779147]

103. Jha V, Kumari T, Manickam V, Assar Z, Olson KL, Min JK, and Cho J (2021). ERO1-PDI Redox Signaling in Health and Disease. Antioxid. Redox Signal. 35, 1093–1115. 10.1089/ars.2021.0018. [PubMed: 34074138]

104. Fernández-Alfara M, Sibilio A, Martin J, Tusquets Uxó E, Malumbres M, Alcalde V, Chanes V, Cañellas-Socias A, Palomo-Ponce S, Batlle E, and Méndez R (2023). Antitumor T-cell function requires CPEB4-mediated adaptation to chronic endoplasmic reticulum stress. EMBO J. 42, e111494. 10.15252/embj.2022111494. [PubMed: 36919984]

105. Liu L, Inoki A, Fan K, Mao F, Shi G, Jin X, Zhao M, Ney G, Jones M, Sun S, et al. (2020). ER-associated degradation preserves hematopoietic stem cell quiescence and self-renewal by restricting mTOR activity. Blood 136, 2975–2986. 10.1182/blood.2020007975. [PubMed: 33150381]

106. Qi L, Tsai B, and Arvan P (2017). New Insights into the Physiological Role of Endoplasmic Reticulum-Associated Degradation. Trends Cell Biol. 27, 430–440. 10.1016/j.tcb.2016.12.002. [PubMed: 28131647]

107. Wei X, Lu Y, Lin LL, Zhang C, Chen X, Wang S, Wu SA, Li ZJ, Quan Y, Sun S, and Qi L (2024). Proteomic screens of SEL1L-HRD1 ER-associated degradation substrates reveal its role in glycosylphosphatidylinositol-anchored protein biogenesis. Nat. Commun. 15, 659. 10.1038/s41467-024-44948-2. [PubMed: 38253565]

108. Xu Y, Zhao F, Qiu Q, Chen K, Wei J, Kong Q, Gao B, Melo-Cardenas J, Zhang B, Zhang J, et al. (2016). The ER membrane-anchored ubiquitin ligase Hrd1 is a positive regulator of T-cell immunity. Nat. Commun. 7, 12073. 10.1038/ncomms12073. [PubMed: 27417417]

109. Hong HS, Mbah NE, Shan M, Loesel K, Lin L, Sajjakulnukit P, Correa LO, Andren A, Lin J, Hayashi A, et al. (2022). OXPHOS promotes apoptotic resistance and cellular persistence in T(H)17 cells in the periphery and tumor microenvironment. Sci. Immunol. 7, eabm8182. 10.1126/sciimmunol.abm8182. [PubMed: 36399539]

110. O'Sullivan D, van der Windt GJW, Huang SCC, Curtis JD, Chang CH, Buck MD, Qiu J, Smith AM, Lam WY, DiPlato LM, et al. (2014). Memory CD8(+) T cells use cell-intrinsic lipolysis to support the metabolic programming necessary for development. Immunity 41, 75–88. 10.1016/j.immuni.2014.06.005. [PubMed: 25001241]

111. Klein Geltink RI, O'Sullivan D, Corrado M, Bremser A, Buck MD, Buescher JM, Firat E, Zhu X, Niedermann G, Caputa G, et al. (2017). Mitochondrial Priming by CD28. Cell 171, 385–397.e311. 10.1016/j.cell.2017.08.018. [PubMed: 28919076]

112. Humblin E, Korpas I, Lu J, Filipescu D, van der Heide V, Goldstein S, Vaidya A, Soares-Schanoski A, Casati B, Selvan ME, et al. (2023). Sustained CD28 costimulation is required for self-renewal and differentiation of TCF-1(+) PD-1(+) CD8 T cells. Sci. Immunol. 8, eadg0878. 10.1126/sciimmunol.adg0878. [PubMed: 37624910]

113. Wang N, Wang C, Zhao H, He Y, Lan B, Sun L, and Gao Y (2021). The MAMs Structure and Its Role in Cell Death. Cells 10, 657. 10.3390/cells10030657. [PubMed: 33809551]

114. Friedman JR, Lackner LL, West M, DiBenedetto JR, Nunnari J, and Voeltz GK (2011). ER tubules mark sites of mitochondrial division. Science 334, 358–362. 10.1126/science.1207385. [PubMed: 21885730]

115. Nava Lauson CB, Tiberti S, Corsetto PA, Conte F, Tyagi P, Machwirth M, Ebert S, Loffreda A, Scheller L, Sheta D, et al. (2023). Linoleic acid potentiates CD8(+) T cell metabolic fitness and antitumor immunity. Cell Metab. 35, 633–650.e9. 10.1016/j.cmet.2023.02.013. [PubMed: 36898381]

116. Bantug GR, Fischer M, Grählert J, Balmer ML, Unterstab G, Develioglu L, Steiner R, Zhang L, Costa ASH, Gubser PM, et al. (2018). Mitochondria-Endoplasmic Reticulum Contact Sites Function as Immunometabolic Hubs that Orchestrate the Rapid Recall Response of Memory CD8(+) T Cells. Immunity 48, 542–555.e6. 10.1016/j.immuni.2018.02.012. [PubMed: 29523440]

117. Yang JF, Xing X, Luo L, Zhou XW, Feng JX, Huang KB, Liu H, Jin S, Liu YN, Zhang SH, et al. (2023). Mitochondria-ER contact mediated by MFN2-SERCA2 interaction supports CD8(+) T cell metabolic fitness and function in tumors. Sci. Immunol. 8, eabq2424. 10.1126/sciimmunol.abq2424. [PubMed: 37738362]

118. Guo A, Huang H, Zhu Z, Chen MJ, Shi H, Yuan S, Sharma P, Connelly JP, Liedmann S, Dhungana Y, et al. (2022). cBAF complex components and MYC cooperate early in CD8(+) T cell fate. Nature 607, 135–141. 10.1038/s41586-022-04849-0. [PubMed: 35732731]

119. Bianchi T, Gasser S, Trumpp A, and MacDonald HR (2006). c-Mycacts downstream of IL-15 in the regulation of memory CD8 T-cell homeostasis. Blood 107, 3992–3999. 10.1182/blood-2005-09-3851. [PubMed: 16449532]

120. Haque M, Song J, Fino K, Wang Y, Sandhu P, Song X, Norbury C, Ni B, Fang D, Salek-Ardakani S, and Song J (2016). C-Myc regulation by costimulatory signals modulates the generation of CD8+ memory T cells during viral infection. Open Biol. 6, 150208. 10.1098/rsob.150208. [PubMed: 26791245]

121. Lindsten T, June CH, and Thompson CB (1988). Multiple mechanisms regulate c-myc gene expression during normal T cell activation. EMBO J. 7, 2787–2794. 10.1002/j.1460-2075.1988.tb03133.x. [PubMed: 3053165]

122. Guy CS, Vignali KM, Temirov J, Bettini ML, Overacre AE, Smeltzer M, Zhang H, Huppa JB, Tsai YH, Lobry C, et al. (2013). Distinct TCR signaling pathways drive proliferation and cytokine production in T cells. Nat. Immunol. 14, 262–270. 10.1038/ni.2538. [PubMed: 23377202]

123. Rodriguez-Otero P, and San-Miguel JF (2022). Cellular therapy for multiple myeloma: what's now and what's next. Hematology 2022, 180–189. 10.1182/hematology.2022000396. [PubMed: 36485132]

124. van de Donk NWCJ, and Zweegman S (2023). T-cell-engaging bispecific antibodies in cancer. Lancet 402, 142–158. 10.1016/S0140-6736(23)00521-4. [PubMed: 37271153]

125. Mackensen A, Muller F, Mougiakakos D, Böltz S, Wilhelm A, Aigner M, Völkl S, Simon D, Kleyer A, Munoz L, et al. (2022). Anti-CD19 CAR T cell therapy for refractory systemic lupus erythematosus. Nat. Med. 28, 2124–2132. 10.1038/s41591-022-02017-5. [PubMed: 36109639]

126. Gumber D, and Wang LD (2022). Improving CAR-T immunotherapy: Overcoming the challenges of T cell exhaustion. EBioMedicine 77, 103941. 10.1016/j.ebiom.2022.103941. [PubMed: 35301179]

127. Kaech SM, and Ahmed R (2001). Memory CD8+ T cell differentiation: initial antigen encounter triggers a developmental program in naive cells. Nat Immunol 2, 415–422. 10.1038/87720. [PubMed: 11323695]

128. Quiros PM, Goyal A, Jha P, and Auwerx J (2017). Analysis of mtDNA/nDNA Ratio in Mice. Curr Protoc Mouse Biol 7, 47–54. 10.1002/cpmo.21. [PubMed: 28252199]

129. Love MI, Huber W, and Anders S (2014). Moderated estimation of fold change and dispersion for RNA-seq data with DESeq2. Genome Biol. 15, 550. 10.1186/s13059-014-0550-8. [PubMed: 25516281]

130. Soneson C, Love MI, and Robinson MD (2015). Differential analyses for RNA-seq: transcript-level estimates improve gene-level inferences. F1000Res 4, 1521. 10.12688/f1000research.7563.2. [PubMed: 26925227]

131. Li B, and Dewey CN (2011). RSEM: accurate transcript quantification from RNA-Seq data with or without a reference genome. BMC Bioinf. 12, 323. 10.1186/1471-2105-12-323.

132. Dobin A, Davis CA, Schlesinger F, Drenkow J, Zaleski C, Jha S, Batut P, Chaisson M, and Gingeras TR (2013). STAR: ultrafast universal RNA-seq aligner. Bioinformatics 29, 15–21. 10.1093/bioinformatics/bts635. [PubMed: 23104886]

133. Martin M (2011). Cutadapt Removes Adapter Sequences from High-Throughput Sequencing Reads. EMBnet J. 17, 3. 10.14806/ej.17.1.200.

134. Ewels P, Magnusson M, Lundin S, and Käller M (2016). MultiQC: summarize analysis results for multiple tools and samples in a single report. Bioinformatics 32, 3047–3048. 10.1093/bioinformatics/btw354. [PubMed: 27312411]

135. Wolf FA, Angerer P, and Theis FJ (2018). SCANPY: large-scale single-cell gene expression data analysis. Genome Biol. 19, 15. 10.1186/s13059-017-1382-0. [PubMed: 29409532]

136. Badia-I-Mompel P, Vélez Santiago J, Braunger J, Geiss C, Dimitrov D, Müller-Dott S, Taus P, Dugourd A, Holland CH, Ramirez Flores RO, and Saez-Rodriguez J (2022). decoupleR: ensemble of computational methods to infer biological activities from omics data. Bioinform. Adv. 2, vbac016. 10.1093/bioadv/vbac016. [PubMed: 36699385]

137. Hänzelmann S, Castelo R, and Guinney J (2013). GSVA: gene set variation analysis for microarray and RNA-seq data. BMC Bioinf. 14, 7. 10.1186/1471-2105-14-7.

138. Tyanova S, Temu T, Sinitcyn P, Carlson A, Hein MY, Geiger T, Mann M, and Cox J (2016). The Perseus computational platform for comprehensive analysis of (prote)omics data. Nat Methods 13, 731–740. 10.1038/nmeth.3901. [PubMed: 27348712]

139. Korotkevich G, Sukhov V, Budin N, Shpak B, Artyomov MN, and Sergushichev A (2021). Fast gene set enrichment analysis. Preprint at bioRxiv. 10.1101/060012.

140. Wickham H, McGowan LDA, et al. (2019). Welcome to the Tidyverse. The Journal of Open Source Software. 10.21105/joss.01686.

141. Ewels PA, Peltzer A, Fillinger S, Patel H, Alneberg J, Wilm A, Garcia MU, Di Tommaso P, and Nahnsen S (2020). The nf-core framework for community-curated bioinformatics pipelines. Nat. Biotechnol. 38, 276–278. 10.1038/s41587-020-0439-x. [PubMed: 32055031]

142. Stirling DR, Swain-Bowden MJ, Lucas AM, Carpenter AE, Cimini BA, and Goodman A (2021). CellProfiler 4: improvements in speed, utility and usability. BMC Bioinf. 22, 433. 10.1186/s12859-021-04344-9.

143. Pircher H, Baenziger J, Schilham M, Sado T, Kamisaku H, Hengartner H, and Zinkernagel RM (1987). Characterization of virus-specific cytotoxic T cell clones from allogeneic bone marrow chimeras. Eur. J. Immunol. 17, 159–166. 10.1002/eji.1830170202. [PubMed: 3493906]

144. Pircher H, Michalopoulos EE, Iwamoto A, Ohashi PS, Baenziger J, Hengartner H, Zinkernagel RM, and Mak TW (1987). Molecular analysis of the antigen receptor of virus-specific cytotoxic T cells and identification of a new V alpha family. Eur. J. Immunol. 17, 1843–1846. 10.1002/eji.1830171226. [PubMed: 2961577]

145. Carty SA, Gohil M, Banks LB, Cotton RM, Johnson ME, Stelekati E, Wells AD, Wherry EJ, Koretzky GA, and Jordan MS (2018). The Loss of TET2 Promotes CD8(+) T Cell Memory Differentiation. J. Immunol. 200, 82–91. 10.4049/jimmunol.1700559. [PubMed: 29150566]

146. Hitz BC, Jolanki O, Kagda MS, Graham K, Sud P, Gabdank I, Seth Strattan J, Sloan CA, Dreszer T, Rowe LD, et al. (2023). The ENCODE Uniform Analysis Pipelines. Preprint at bioRxiv. 10.1101/2023.04.04.535623.

147. Fogo GM, Anzell AR, Maheras KJ, Raghunayakula S, Wider JM, Emaus KJ, Bryson TD, Bukowski MJ, Neumar RW, Przyklenk K, and Sanderson TH (2021). Machine learning-based classification of mitochondrial morphology in primary neurons and brain. Sci. Rep. 11, 5133. 10.1038/s41598-021-84528-8. [PubMed: 33664336]

148. Schindelin J, Arganda-Carreras I, Frise E, Kaynig V, Longair M, Pietzsch T, Preibisch S, Rueden C, Saalfeld S, Schmid B, et al. (2012). Fiji: an open-source platform for biological-image analysis. Nat. Methods 9, 676–682. 10.1038/nmeth.2019. [PubMed: 22743772]

149. Arganda-Carreras I, Kaynig V, Rueden C, Eliceiri KW, Schindelin J, Cardona A, and Sebastian Seung H (2017). Trainable Weka Segmentation: a machine learning tool for microscopy pixel classification. Bioinformatics 33, 2424–2426. 10.1093/bioinformatics/btx180. [PubMed: 28369169]

150. Legland D, Arganda-Carreras I, and Andrey P (2016). MorphoLibJ: integrated library and plugins for mathematical morphology with ImageJ. Bioinformatics 32, 3532–3534. 10.1093/bioinformatics/btw413. [PubMed: 27412086]

151. Ollion J, Cochennec J, Loll F, Escudé C, and Boudier T (2013). TANGO: a generic tool for high-throughput 3D image analysis for studying nuclear organization. Bioinformatics 29, 1840–1841. 10.1093/bioinformatics/btt276. [PubMed: 23681123]

152. Cignoni P, Callieri M, Corsini M, Dellepiane G, Ganovelli F, and Ranzuglia G (2008). MeshLab: an Open-Source Mesh Processing Tool. In Eurographics Italian Chapter Conference. 10.2312/LocalChapterEvents/ItalChap/ItalianChapConf2008/129-136.

153. Liberzon A, Subramanian A, Pinchback R, Thorvaldsdóttir H, Tamayo P, and Mesirov JP (2011). Molecular signatures database (MSigDB) 3.0. Bioinformatics 27, 1739–1740. 10.1093/bioinformatics/btr260. [PubMed: 21546393]

154. Cox J, Hein MY, Luber CA, Paron I, Nagaraj N, and Mann M (2014). Accurate proteome-wide label-free quantification by delayed normalization and maximal peptide ratio extraction, termed MaxLFQ. Mol. Cell. Proteomics 13, 2513–2526. 10.1074/mcp.M113.031591. [PubMed: 24942700]

Highlights

- Virus-specific $CD8^+$ T cells experience ER stress during an acute viral infection
- Sel1L/ERAD is required for $CD8^+$ T cell function and persistence
- Sel1L/ERAD supports T cell oxidative phosphorylation and c-Myc expression

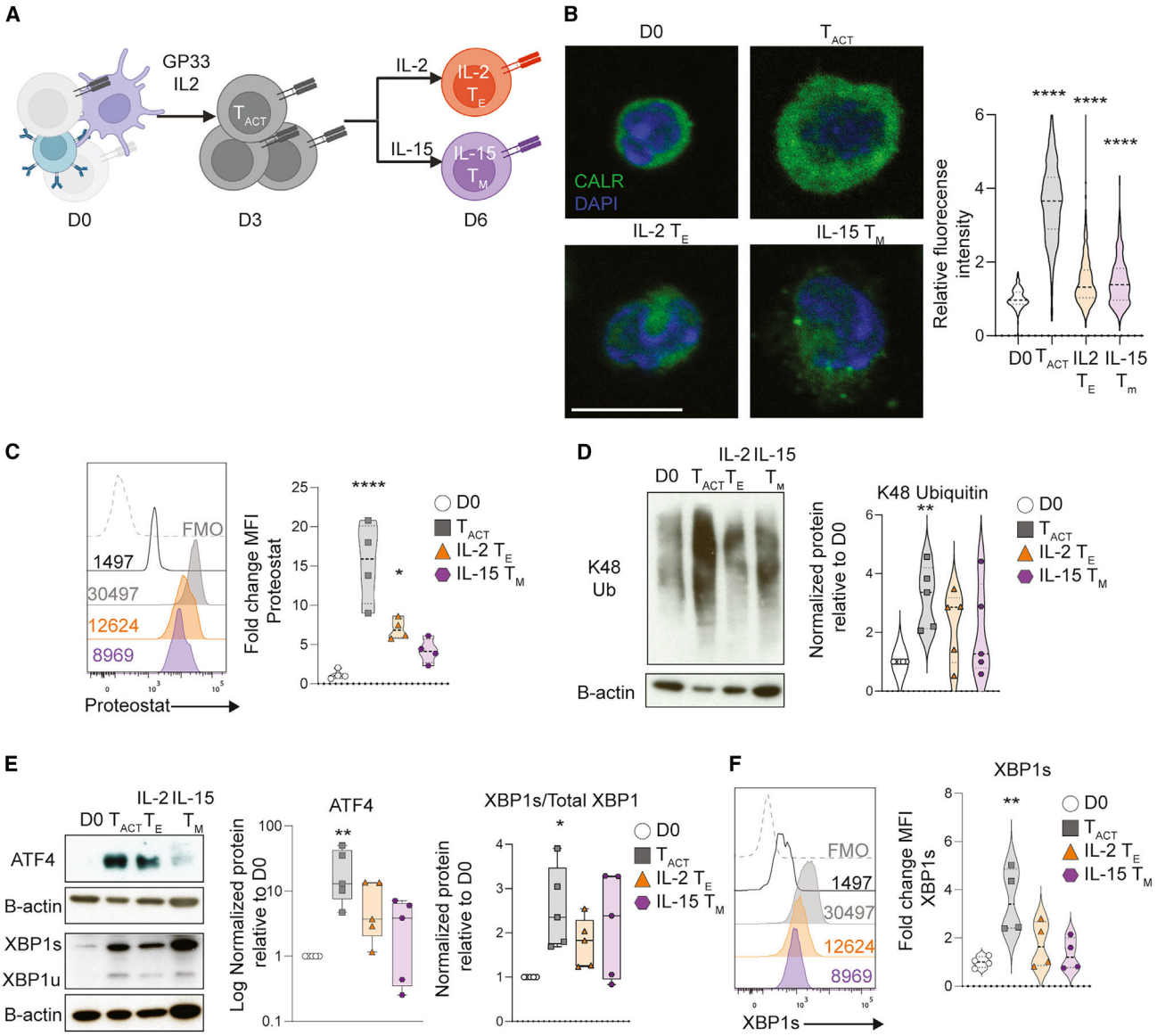

Figure 1. T cell activation induces ER stress *in vitro*

(A) Experimental schema. Splenocytes from wild-type (WT) P14 transgenic mice were activated *in vitro* with LCMV gp33–41 peptide in the presence of IL-2 for 3 days (T_{ACT}), then incubated with either IL-2 to generate IL-2 "effector" cells (IL-2 T_E) or IL-15 to generate IL-15 "memory" cells (IL-15 T_M). Created with BioRender.com.

(B) (Left) Confocal microscopy and (right) associated quantification of calreticulin (CALR) in *in vitro* naive (D0), T_{ACT} (D3), IL-2 T_E, and IL-15 T_M P14 cells. Scale bar represents 10 μm.

(C) (Left) Representative histograms of PROTEOSTAT in *in vitro* naive (D0), T_{ACT}, IL-2 T_E, and IL-15 T_M. (Right) Fold change in median fluorescence intensity (MFI) of PROTEOSTAT normalized to naive.

(D) (Left) Representative immunoblot of K48-Ub in serially collected *in vitro* naive, T_{ACT}, IL-2 T_E, and IL-15 T_M P14 cells. (Right) Densitometry quantification of the K48-Ub immunoblot bands in indicated conditions.

(E) (Left) Representative immunoblot of ATF4 and XBP1 (spliced/unspliced) in serially collected *in vitro* naive, T_{ACT}, IL-2 T_E, and IL-15 T_M P14 cells. (Right) Densitometry quantification of the immunoblot bands.

(F) (Left) Representative histograms of XBP1s in *in vitro* naive, T_{ACT}, IL-2 T_E, and IL-15 T_M. (Right) Fold change in MFI of XBP1s normalized to naive. Data representative of naive $n = 276$, T_{ACT} $n = 376$, IL-2 T_E $n = 882$, and IL-15 T_M $n = 751$ (B), $n = 4$ (C and F), and $n = 5$ (D and E). All immunoblot data are normalized β-actin, then to naive. $*p < 0.05$, $**p < 0.01$, $****p < 0.0001$, one-way ANOVA with uncorrected Fisher's least significant difference (B–F).

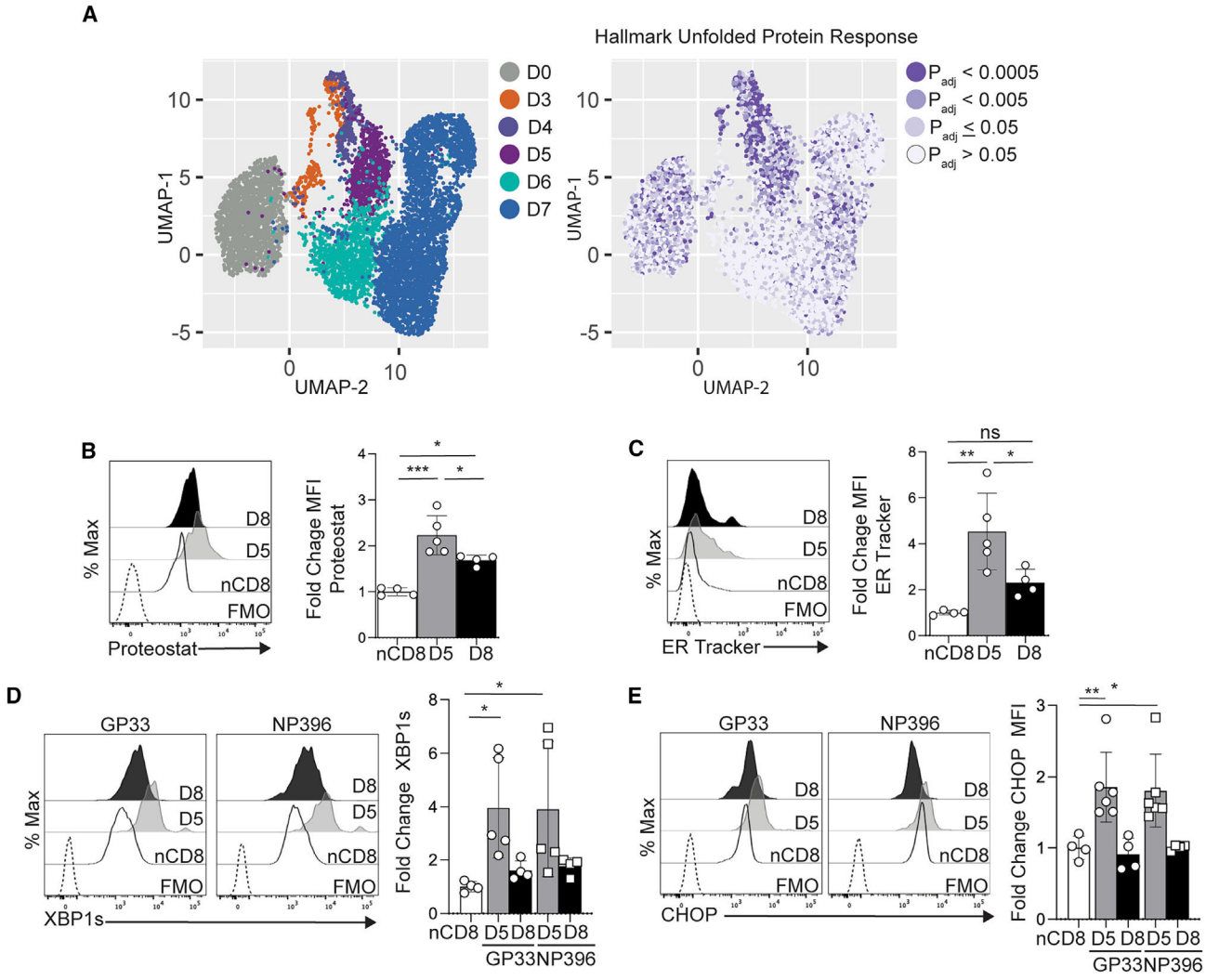

Figure 2. Antigen-specific CD8$^+$ T cells experience dynamic ER stress during an acute viral infection *in vivo*

(A) (Left) Uniform manifold approximation and projection (UMAP) of P14 cells responding to LCMV infection (GEO: GSE131847) determined by scanpy. Each dot corresponds to one individual cell colored by day of infection. (Right) enrichment (adjusted p values) of gene module “hallmark unfolded protein response” determined by Fisher’s exact test (decouplr) and used to color UMAP plots.

(B and C) (Left) Representative histograms of PROTEOSTAT (B) or ER Tracker (C) in gp33$^+$CD44$^+$CD8$^+$TCRb$^+$ splenocytes isolated on indicated days post infection (p.i.). LCMV compared to naive CD8$^+$ T cells from uninfected mice. (Right) Fold change in MFI of PROTEOSTAT or ER Tracker normalized to uninfected naive CD8$^+$ T cells.

(D and E) (Left) Representative histograms of intracellular XBP1s (D) and intracellular CHOP (E) in gp33$^+$ or NP396$^+$CD44$^+$CD8$^+$TCRb$^+$ splenocytes. (Right) Fold change in MFI of XBP1s (D) or CHOP (E) in gp33$^+$ or NP396$^+$ normalized to uninfected naive CD8$^+$ T cells. Fluorescence minus one (FMO) depicted as negative control in histograms.

Data are representative of $n = 4–6$ from two independent experiments. *$p < 0.05$, **$p < 0.01$, ***$p < 0.001$; ns, not significant (p R 0.5); one-way ANOVA with Dunnett's multiple comparison test. Data are shown as mean ± SD.

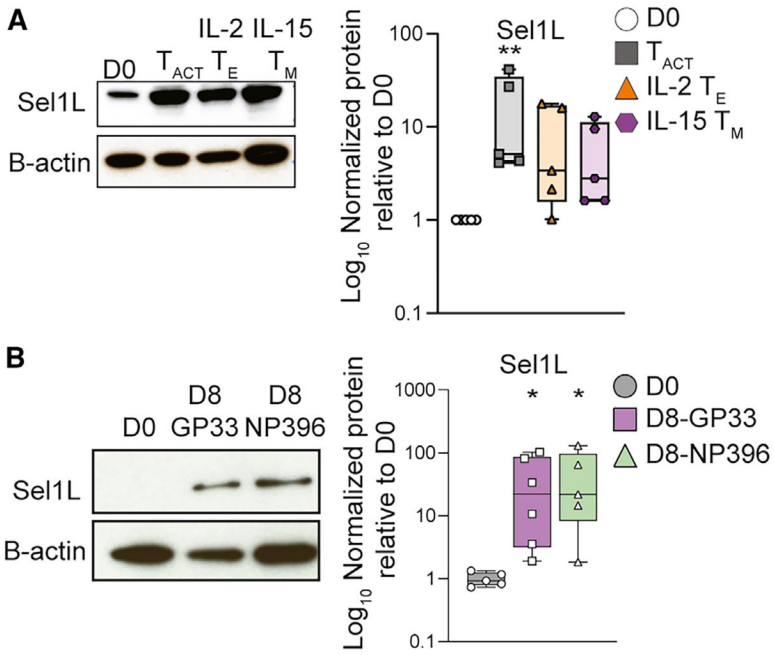

Figure 3. Sel1L is induced in antigen-experienced cells

(A) (Left) Representative immunoblot of Sel1L and β-actin in serially collected *in vitro* naive, T_{ACT}, IL-2 T_E, and IL-15 T_M cells (10 mg lysates). (Right) Densitometry quantification of the immunoblot band normalized to β-actin.

(B) (Left) Representative immunoblot of uninfected naive $CD8^+$ T cells and $gp33^+$ and $NP396^+$ $CD8^+$ T cells (2×10^5 cells) from mice on day 8 (D8) with LCMV. (Right) Densitometry quantification of the immunoblot band normalized to β-actin.

Data are representative of $n = 5–6$ from two independent experiments. $^*p < 0.05$, $^{**}p < 0.01$, Friedman test with Dunnett's multiple comparisons test (A) and Kruskal-Wallis test with Dunnett's multiple comparisons test (B).

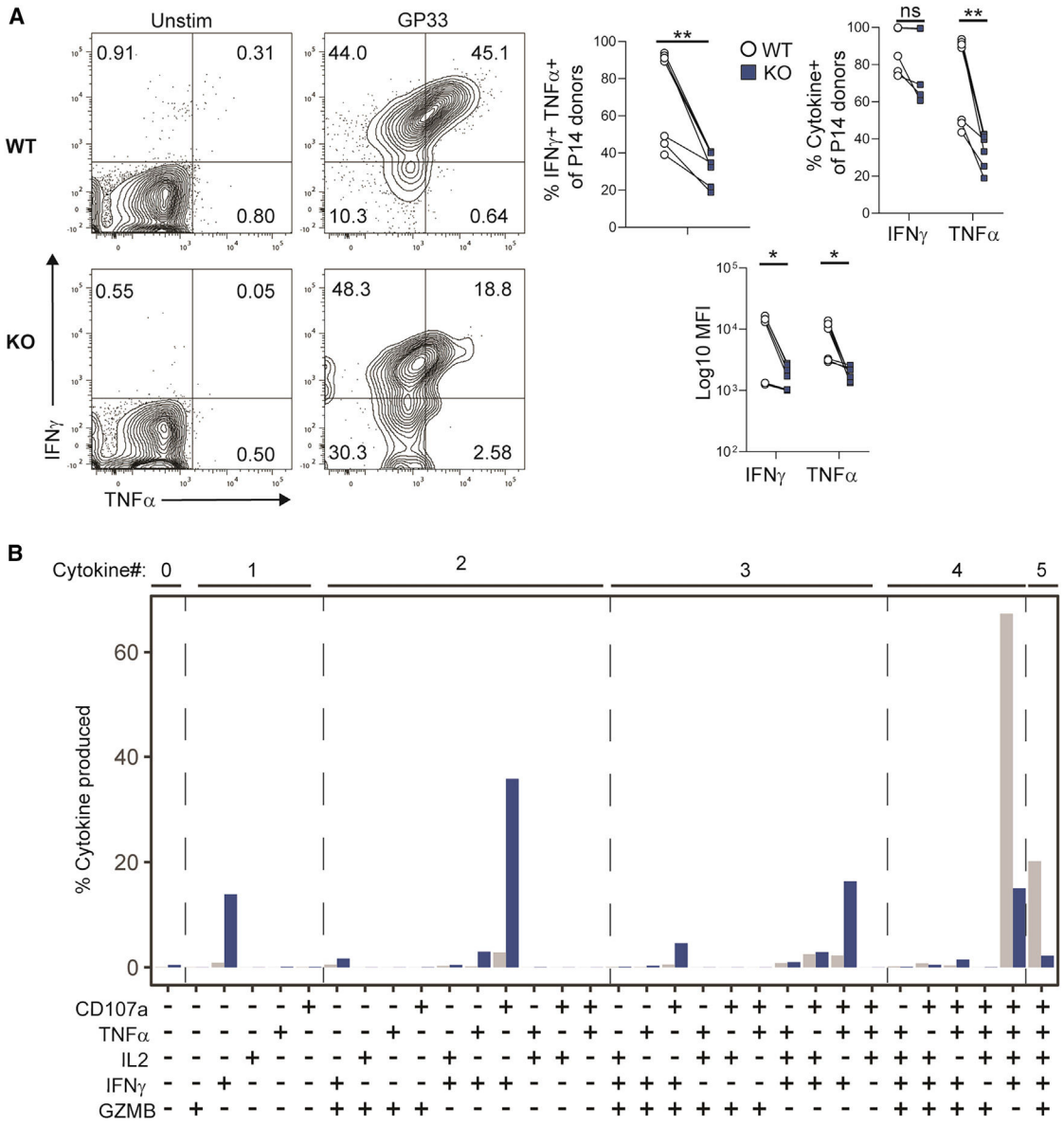

Figure 4. Sel1L/ERAD is required for optimal CD8$^+$ T cell effector function

Peripheral blood lymphocytes from Sel1LcKO P14 (CD45.2) and WT P14 (CD45.1/2) mice were mixed to generate a 1:1 mix of donor P14 cells, which was subsequently transferred into B6.SJL (CD45.1) mice. These mice were infected with LCMV-Armstrong the following day. At day 8 p.i., splenocytes were stimulated ex vivo with gp33 peptide.

(A) Representative plots of intracellular TNF-α and IFN-γ expression (left) and frequencies (top right) of indicated cell populations in donor P14 cells, as well as MFI of indicated cytokine among cytokine$^+$ populations (bottom right).

(B) Cytokine co-expression in ex vivo restimulated WT or KO P14 cells at day 8 p.i. Dashed lines separate columns by number of cytokines produced.

Data are representative of $n = 8$/genotype from two independent experiments. *$p < 0.05$, **$p < 0.01$; ns, not significant; paired t test.

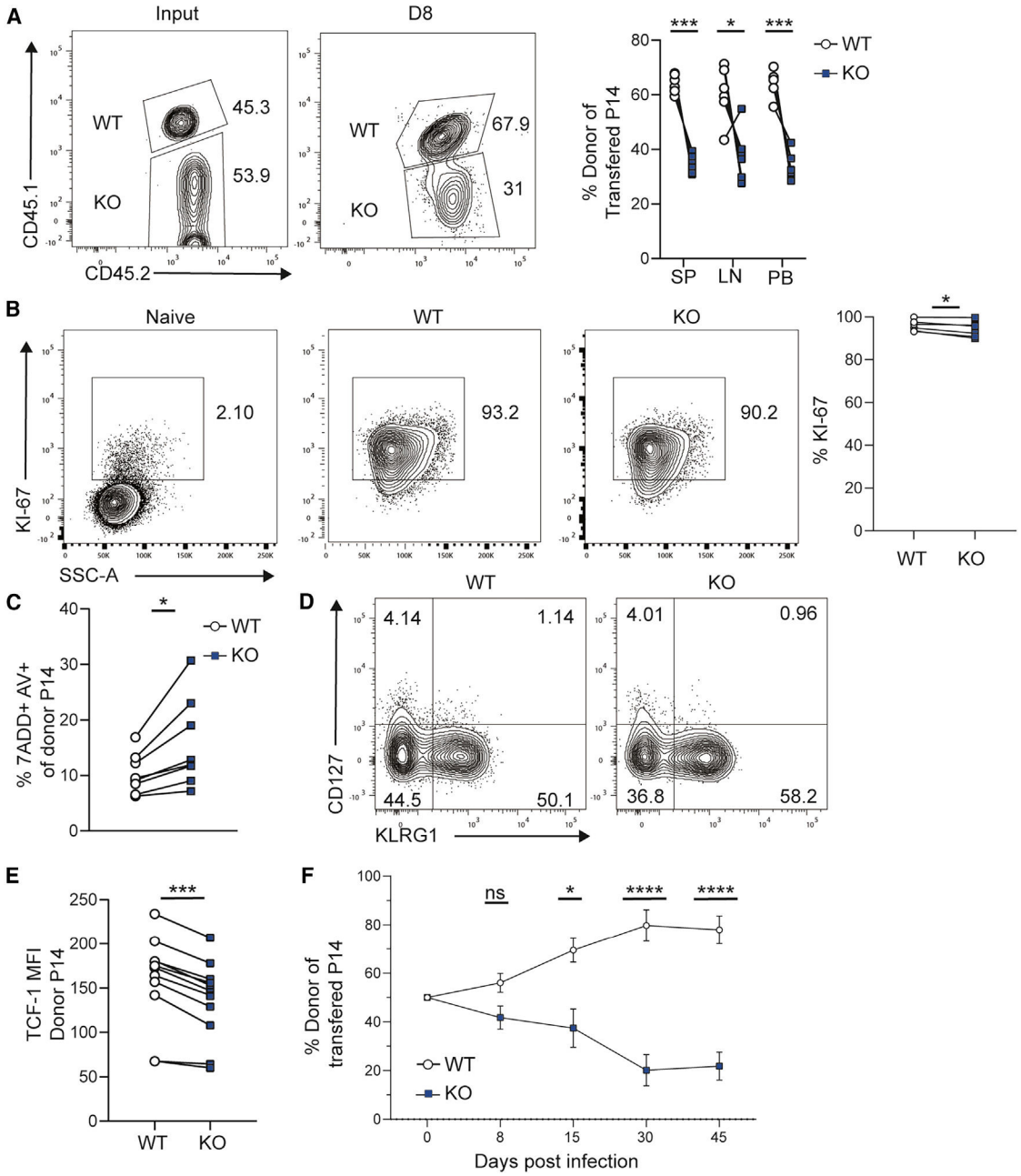

Figure 5. Sel1L/ERAD is required for CD8$^+$ T cell survival and memory formation

Sel1LcKO P14 (CD45.2) and WT P14 (CD45.1/2) cells were mixed 1:1 and adoptively co-transferred into B6.SJL (CD45.1) mice, which were infected with LCMV-Armstrong the following day. Flow-cytometric analysis of donor P14 cells was performed on day 8 (D8; A–E) and peripheral blood mononuclear cells (PBMCs) serially collected (F).

(A) (Left) Representative flow-cytometric analysis of donor P14 input and at D8 p.i. (center). (Right) Donor frequencies of indicated genotypes in spleen (SP), lymph nodes (LN), and peripheral blood (PB).

(B) (Left) Representative flow-cytometric analysis of Ki67 in naive CD8$^+$ T cells as negative control and donor P14. (Right) Frequency of Ki67$^+$ population in donor P14 cells.

(C) Frequency of $7AAD^+$ Annexin V $(AV)^+$ populations among donor P14.
(D) Representative flow-cytometric analysis of CD127 and KLRG1 expression in donor P14 cells.
(E) MFI of TCF-1 in donor P14 populations.
(F) Frequency of indicated genotypes among donor P14 cells in PBMCs at indicated time points ± SEM.
Data are representative of $n = 6$/genotype from two independent experiments (A and B); $n = 8$/genotype from two independent experiments (C); $n = 5–9$ from 2–3 independent experiments (D); $n = 11$ from three independent experiments (E); $n = 12$ from three independent experiments (F). *$p < 0.05$, **$p < 0.01$, ***$p < 0.001$, ****$p < 0.0001$; ns, not significant ($p > 0.05$); paired t test.

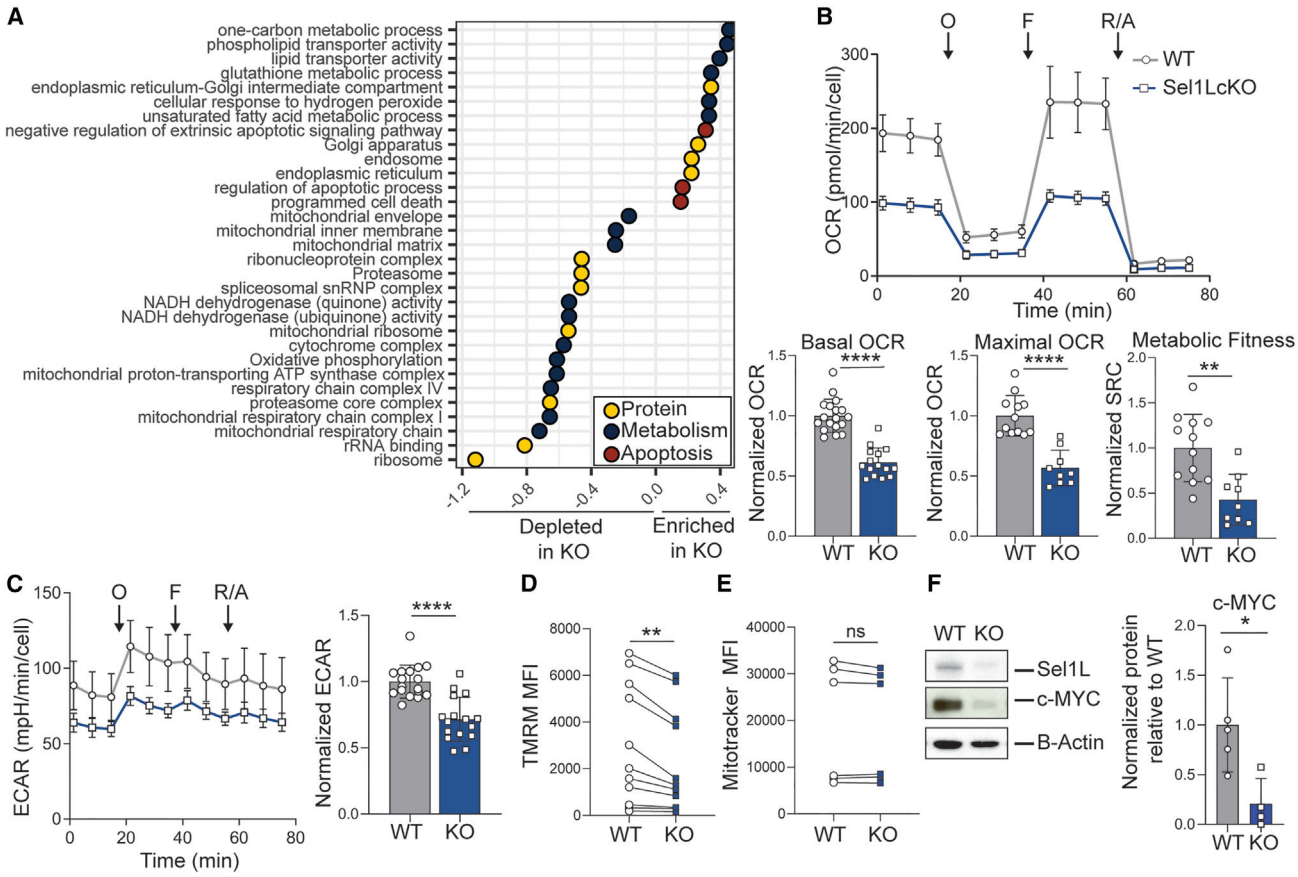

Figure 6. Sel1L/ERAD regulates CD8$^+$ T cell metabolism

(A) Pathway analysis of pathways significantly altered (false discovery rate <0.05) in Sel1LcKO P14 relative to WT P14 transcriptome at day 8 p.i.

(B) Extracellular flux analysis of activated Sel1LcKO P14 and WT P14 cells to assess OXPHOS activity including basal oxygen consumption rate (OCR), maximalOCR, and metabolic fitness as measured by spare respiratory capacity (SRC).

(C) Extracellular flux analysis of activated Sel1LcKO P14 and WT P14 quantifying basal extracellular acidification rate (ECAR).

(D and E) MFI of TMRM (D) or MitoTracker green (E) in Sel1LcKO P14 and WT P14 cells at day 8 p.i.

(F) (Left) Representative immunoblot of Sel1L, c-Myc, and β-actin in WT and KO CD8$^+$ T_{ACT} and (right) densitometry quantification of the c-Myc immunoblot bands in indicated conditions normalized to β-actin, then to WT.

Data are representative of n = 3/genotype from one independent experiment (A), n = 3/genotype from three independent experiments (B and C), n = 7/genotype from two independent experiments (D), n = 12/genotype from three independent experiments (E), and n = 5 WT, n = 4 KO from two independent experiments (F). *p < 0.05, **p < 0.01, ****p < 0.0001; ns, not significant (p > 0.05); unpaired t test (B, C, and F) or paired t test (D and E). Data are shown as mean ± SD. (B, C, and F)

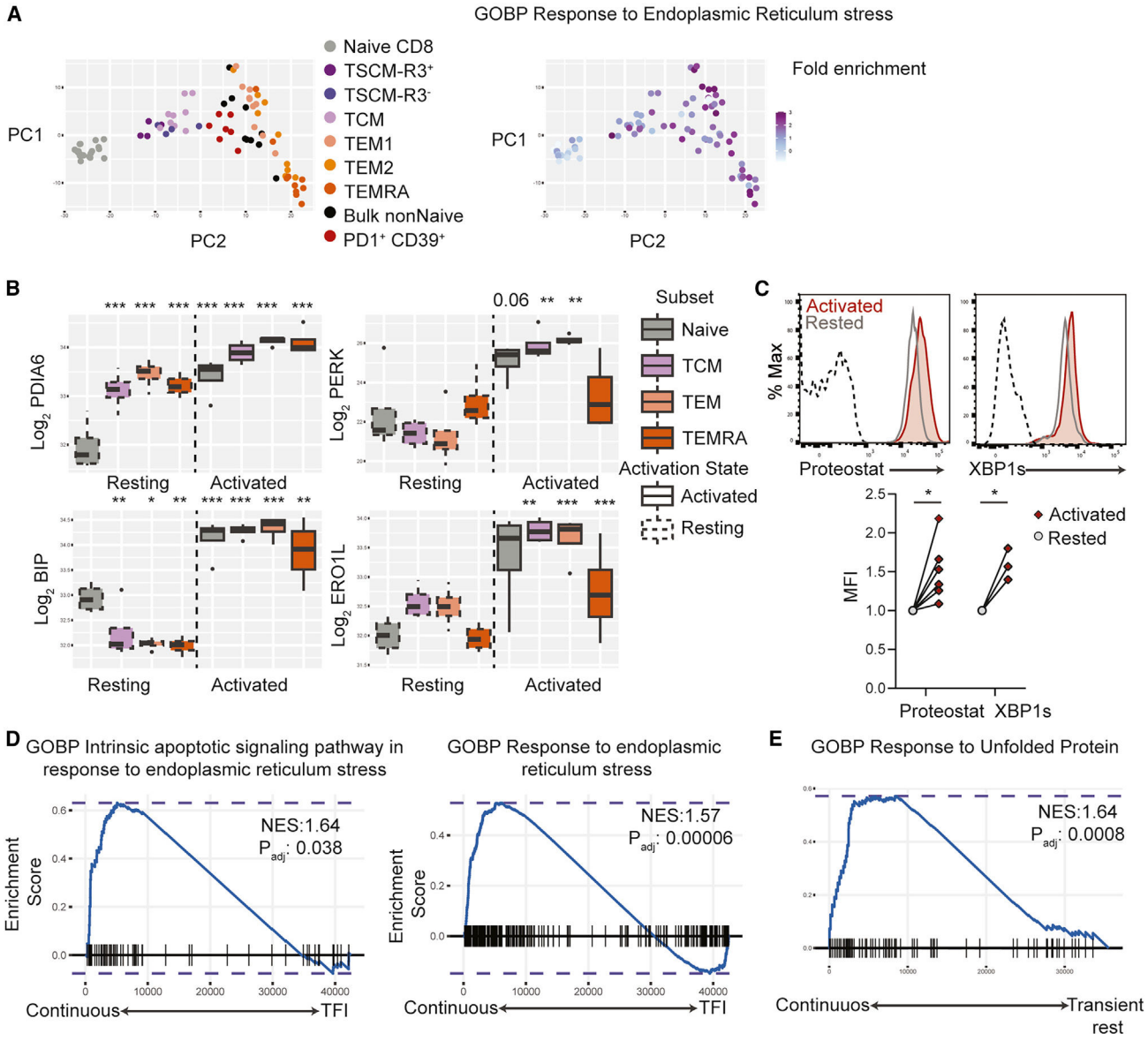

Figure 7. Human CD8$^+$ T cells experience of ER stress is associated with terminal differentiation and reduced persistence

(A) (Left) Principal component (PC) analysis of human CD8$^+$ T cell transcriptomes from peripheral blood of healthy donors from GSE179613. (Right) PC analysis from left colored by fold enrichment of genetic signature (GSVA) “GOBP response to endoplasmic reticulum stress” relative to naive cells.

(B) Log_2 intensity of representative ER stress markers PDIA6, PERK, BiP, and ERO1L in indicated subset and activation state from human CD8$^+$ T cell proteomes from PXD004352.

(C) Representative flow cytometry histograms of (top) PROTEOSTAT and XBP1s MFI and (bottom) PROTEOSTAT and XBP1s in CD8$^+$CD3$^+$ cells from healthy human donors 3 days after activation with CD3/CD28 Dynabeads + IL-2 or rested in IL-7.

(D) Leading-edge plots of gene set enrichment analysis (GSEA) of human T cells undergoing continuous stimulation from bispecific CD3xCD19 (AMG 562) T cells versus cells that experienced a treatment-free interval (TFI) at day 15 from GEO: GSE196463. (E) Leading-edge plots of GSEA of continuously stimulated GD2 CAR-T cells versus transiently rested cells at day 15 from GEO: GSE164950. $n = 7–11$/subset (A), $n = 4$/subset (B), $n = 6$ PROTEOSTAT, $n = 3$ XBP1s (C) from 2–3 independent experiments; $n = 3$/group (D), $n = 3$/group (E). *$p < 0.05$, **$p < 0.01$, ***$p < 0.001$, ****$p < 0.0001$; ns, not significant ($p > 0.05$); unpaired t test (B) or paired t test (C).

KEY RESOURCES TABLE

REAGENT or RESOURCE	SOURCE	IDENTIFIER
Antibodies		
Beta-actin (Clone AC-15)	Sigma	Cat. #A5441-.2ML; RRID:AB_476744
Calreticulin (Polyclonal)	Thermo Scientific	Cat. #PA3900; RRID:AB_325990
XBPIs (Clone E9V3E)	Cell Signaling Technologies	Cat. #40435S; RRID: AB_2891025
c-Myc (Clone D84C12)	Cell Signaling Technologies	Cat. #5605S; RRID:AB_1903938
Opal (Clone D6U6N)	Cell Signaling Technologies	Cat. #80471S; RRID:AB_2734117
Drp1 (Clone D6C7)	Cell Signaling Technologies	Cat. #8570S; RRID:AB_10950498
phosphoDrp1(Ser616) (Polyclonal)	Cell Signaling Technologies	Cat. #3455S; RRID:AB_2085352
K48-Ub (Clone D9D5)	Cell Signaling Technologies	Cat. #8081S; RRID:AB_10859893
XBP1 (Polyclonal)	Novus Biologicals	Cat. #NBP1– 77681; RRID:AB_11010815
ATF4 (Clone D4B8)	Cell Signaling Technologies	Cat. #11815S; RRID:AB_2616025
Sel1L (Polyclonal)	Abcam	Cat. #ab78298; RRID:AB_2285813
CHOP (Clone L63F7)	Cell Signaling Technologies	Cat. # 2895T; RRID:AB_2089254
ATPB (Clone 3D5)	Abcam	Cat. #ab14730; RRID:AB_301438
KDEL (Clone EPR12668)	Abcam	Cat.# ab176333; RRID:AB_2819147
TOM20 (Clone 4F3)	Abcam	Cat.# ab56783; RRID:AB_945896
CD44 AF700 (Clone IM7)	Biolegend	Cat.# 103026; RRID:AB_493713
TCRb APC-Cy7 (Clone H57–597)	Biolegend	Cat. # 109220; RRID:AB_893624
CD8a Pacific Blue (Clone 53–6.7)	Biolegend	Cat. # 100725; RRID:AB_493425
CD127 PE-Cy7 (Clone A7R34)	Biolegend	Cat. # 135014; RRID:AB_1937265
CD62L PE-Texas-Red (Clone MEL-14)	Biolegend	Cat. # RM4317; RRID:AB_1479970
CD25 AF488 (Clone PC61)	Biolegend	Cat. # 102017; RRID:AB_493334
CD69 APC (Clone H1.2F3)	Biolegned	Cat. # 104514; RRID:AB_492843
CD45.1 PerCP-Cy5.5 (Clone A20)	eBiosciences	Cat. # 45-0453-80; RRID:AB_925750
CD45.1 BV650 (Clone A20)	Biolegend	Cat. # 110736; RRID:AB_2562564
CD45.1 AF700 (Clone A20)	Biolegend	Cat. # 110724; RRID:AB_493733
CD45.2 PE (Clone 104)	Biolegend	Cat. # 109808; RRID:AB_313445
CD45.2 Pacific Blue (Clone 104)	Biolegend	Cat. # 109820; RRID:AB_492873
IFNg PerCP-Cy 5.5 (Clone XMG1.2)	Biolegend	Cat. # 505822; RRID:AB_961361
TNFa BV421 (Clone MP6-XT22)	Fisher Scientific	Cat. # BDB563387; RRID:AB_2925546
IL2 PE (Clone JES6-5H4)	Fisher Scientific	Cat. # BDB554429; RRID:AB_398555
Granzyme B PE-Cy7 (Clone NGZB)	Fisher Scientific	Cat. # 50-245-758; RRID:AB_10853338
CD107a FITC (Clone 1D4B)	Fisher Scientific	Cat. # 121606; RRID:AB_572006
KLRG1 FITC (Clone 2F1)	Fisher Scientific	Cat.# 50-990-3; RRID:AB_1311265
Ki-67 (Clone B56)	Fisher Scientific	Cat. # BDB556026; RRID:AB_396302

REAGENT or RESOURCE	SOURCE	IDENTIFIER
TCF1 (Clone C63D9)	Cell Signaling Technologies	Cat. # 14456S; RRID:AB_2798483
Goat anti-Mouse AF488 (Polyclonal)	Thermo Fisher Scientific	Cat. # A-11029; RRID:AB_2534088
Goat anti-Mouse AF594 (Polyclonal)	Thermo Fisher Scientific	Cat.# A-11005; RRID:AB_2534073
Goat anti-Rabbit 488 (Polyclonal)	Thermo Fisher Scientific	Cat.# A-11034; RRID: AB_2576217
Bacterial and virus strains		
Listeria monocytogenes-gp33	Kaech et al.[127]	N/A
Lymphocytic choriomeningitis Virus - Armstrong strain	Rafi Ahmed	Grown by Wherry lab
Chemicals, peptides, and recombinant proteins		
2-Mercaptoethanol	Sigma-Aldrich	Cat. #M3148-250ML
Ficoll-paque	GE Healthcare	Cat.# 45-001-749
RIPA Buffer	Pierce	Cat.# PI89900
Protease Inhibitor	Thermo Scientific	Cat.# 1862495
Halt Phosphatase Inhibitor	Thermo Scientific	Cat.# 1862209
gp33–41 (KAVYNFATC)	Anaspec	Cat.# AS-61669
hIL-2	PeproTech	Cat.# 200-02
mIL-15	PeproTech	Cat.# 210-15
human IL-7	PeproTech	Cat. #200-07-10ug
BD Cytofix/cytoperm kit	BD Biosciences	Cat.# BDB554722
Foxp3/transcription factor staining buffer	Invitrogen	Cat.# 50-112-8857
Seahorse Mitostress kit	Agilent	Cat. #103015-100
Critical commercial assays		
PROTEOSTAT	Enzo	Cat.# ENZ-51023-KP002
DAPI	Sigma-Aldrich	Cat. #D9542-1MG
ER Tracker	Thermo Scientific	Cat.#E34250
gp33 $H2D^b$ Tetramer	NIH Tetramer Core	N/A
NP396 $H2D^b$ Tetramer	NIH Tetramer Core	N/A
tetramethylrhodamine methyl ester perchlorate (TMRM)	Thermo Fisher Scientific	Cat. #T668
Mitotracker Green	Thermo Fisher Scientific	Cat. #M7514
Deposited data		
scRNA-seq: Mus musculus P14 $CD8^+$ T cells from LCMV-Armstrong infected mice	Kurd et al.[52]	GSE131847
Bulk-RNAseq: Mus musculus WT or Sel1LcKO P14 $CD8^+$ T cell from LCMV-Armstrong infected mice	This paper	GSE244315
Bulk-RNAseq: Human $CD8^+$ T cells	Giles et al.[92]	GSE179613
Bulk-RNAseq: Human T cells	Philipp et al.[99]	GSE196463
Bulk-RNAseq: Human GD2 CAR-T cells	Weber et al.[100]	GSE164950
Proteomics: Human $CD8^+$ T cells	Rieckmann et al.[93]	PXD004352

REAGENT or RESOURCE	SOURCE	IDENTIFIER
Experimental models: Organisms/strains		
C57BL/6J	The Jackson Laboratories	Cat.# 000664; RRID:IMSR_JAX:000664
CD4Cre+	The Jackson Laboratories	Cat.# 022071: IMSR_JAX:022071
B6.SJL-Ptprca (CD45.1+)	The Jackson Laboratories	Cat.#002014; RRID:IMSR_JAX:002014
P14 mice	The Jackson Laboratories	Cat.# 037394-JAX; RRID: MMRRC_037394-JAX
Sel1L fl/fl mice	Ling Qi lab[25]	N/A
C57BL/6J	The Jackson Laboratories	Cat.# 000664; RRID:IMSR_JAX:000664
Oligonucleotides		
RT-PCR Primer: LCMV-GP Forward (5'GCAACTGCTGTG TTCCCGAAAC)	McCausland et al.[57]	N/A
RT-PCR Primer: LCMV-GP Reverse (5'CATTCACCTGGACTTTGTCAGACTC)	McCausland et al.[57]	N/A
RT-PCR Primer: Mouse-16s Forward (5'CCGCAAGGGAAAGATGAAAGAC)	Quiros et al.[128]	N/A
RT-PCR Primer: Mouse-16s Reverse (5'TCGTTTGGTTTCGGGGTTTC)	Quiros et al.[128]	N/A
RT-PCR Primer: Mouse-Sel1L Forward (5'TGAATCACACCAAAGCCCTG)	Liu et al.[29]	N/A
RT-PCR Primer: Mouse-Sel1L Reverse (5' GCGTAGAGAAAGCCAAGACC)	Liu et al.[29]	N/A
Software and algorithms		
FlowJo 10.10	BD	RRID:SCR_008520
Prism 10.0	GraphPad	RRID:SCR_002798
deseq2 1.38.3	Love et al.[129]	RRID:SCR_015687
Tximport 1.26.1	Soneson et al.[130]	RRID:SCR_016752
r-base 4.2.3	The R foundation	https://www.r-project.org/
python 3.11.3		N/A
FASTQC 0.11.9	N/A	https://www.bioinformatics.babraham.ac.uk/projects/fastqc/:RRID:SCR_014583
Rsem 1.3.1	Li et al.[131]	10.1186/1471-2105-12-323: RRID:SCR_013027
STAR 2.7.10a	Dobin et al.[132]	https://doi.org/10.1093/bioinformatics/bts635: RRID:SCR_004463
RNA-Enrich 1	Lee et al.[70]	RID:SCR_004463
Cutadapt 3.4	Marcel et al.[133]	RRID:SCR_011841
multiQC 1.14	Ewels et al.[134]	https://doi.org/10.1093/bioinformatics/btw354: RRID:SCR_014982
scanpy 1.9.1	Wolf et al.[135]	https://doi.org/10.1186/s13059-017-1382-0:RRID:SCR_018139
Decoupler v1.1	Badia et al.[136]	N/A
SRATools 2.8.2	NCBI	https://hpc.nih.gov/apps/sratoolkit.html:
GSVA 1.46	Hezelman et al.[137]	RRID:SCR_021058

REAGENT or RESOURCE	SOURCE	IDENTIFIER
Perseus 2.0.10.0	Tyanova et al.[138]	RRID:SCR_015753
fgsea 1.24	Korotkevich et al.[139]	RRID:SCR_020938
Tidyverse 2.0	Wickham et al.[140]	RRID:SCR_019186
Conda 4.12.0	Anaconda	RRID:SCR_018317
nf-core/rnas-seq 3.12.0	Ewels et al.[141]	RRID:SCR_024135
Zeiss Zen	Zeis	RRID:SCR_013672
Imaris	Oxford Instruments	RRID:SCR_007370
CellProfiler	Stirling et al.[142]	RRID:SCR_007358
SPICE v6	Roederer et al.[60]	RRID:SCR_016603
Other		
BD Fortessa	BD	N/A
XF-96 Extracellular Flux Analyzer	Agilent	N/A
Nova-seq	Illumina	N/A
SepMate tubes	Stemcell Technologies	Cat. #85450
Cyquant	Invitrogen	Cat. #C7026
$CD8^+$ lymphocytes isolation kit	Invitrogen	Cat. #11147D
ECL Film	Fisher Scientific	Cat. # 45-001-508
Femto ECL Substrate	Fisher Scientific	Cat. # PI34095
ECL Substrate	Fisher Scientific	Cat. # PI32209
Tris Glycine Transfer buffer	Fisher Scientific	Cat. # LC3675
Tris glycine Running buffer	Thermo Scientific	Cat. #LC26754
Tris-buffered saline	Bio-Rad	Cat. # 1706435
Brain Heart Infusion Agar	Sigma-Aldrich	Cat. #70138
Brain Heart Infusion Broth	Sigma-Aldrich	Cat. # 53286
Mojosort™ Mouse CD8 T cell Isolation Kit	Biolegend	Cat. # 480008
Brefeldin A	Beckton Dickson	Cat. #BDB555029
LIVE/DEAD Aqua	Invitrogen	Cat. #L34965
Annexin Binding Buffer	Biolegend	Cat. # 422201
Annexin V	Biolegend	Cat. #640918
7AAD	Biolegend	Cat. # 420403
RPMI	Gibco	Cat. #11875093
L-glutamine/penicillin/streptomycin	Gibco	Cat. #10378016
Non-essential amino acids	Gibco	Cat. #11140050
CD3/28 Dynabeads	Invitrogen	Cat. #11131D
Fetal Bovine Serum	Thermo Fisher Scientific	Cat. # SH3039603